Journal of ELECTRONIC MATERIALS, Vol. 49, No. 8, 2020
https://doi.org/10.1007/s11664-020-08178-8

In-Depth Analysis of Structures, Materials, Models, Parameters, and Applications of Organic Light-Emitting Diodes

SHUBHAM NEGI,[1] POORNIMA MITTAL ,[2,4] and BRIJESH KUMAR[3]

1.—Department of Electronics and Communication Engineering, Graphic Era Deemed to be University, Dehradun, India. 2.—Department of Electronics and Communication Engineering, Delhi Technological University, New Delhi, India. 3.—Department of Electronics and Communication Engineering, Madan Mohan Malaviya University of Technology, Gorakhpur, India. 4.—e-mail: poornimamittal@dtu.ac.in

Organic electronics and specifically organic light-emitting diode (OLED) devices based on organic semiconductor materials enable economically viable large-area flexible applications. This review presents a comprehensive and detailed assessment of different aspects related to OLEDs, focusing on the impact of multilayered architectures on device performance, in particular the impact of different layers and architectures to enhance the output from such devices. Furthermore, characteristic parameters, materials, and fabrication methodologies are reviewed in depth to highlight the major advancements related to OLEDs over the years. Mathematical models are important for predicting the internal operation and characteristics of such devices, thus these are also discussed, focusing on methods to improve the performance parameters of OLEDs. Applications of OLEDs are also discussed, with a primary focus on research related to their improvement and enhancement for use in displays, sensors, and visual light communications. Although OLEDs show great promise for a bright future, several challenges such as the development of blue light-emitting materials, lifetime improvement, and application-specific architectures must be addressed to achieve more dynamic devices for emerging commercial applications.

Key words: Organic semiconductor (OSC), organic light-emitting diode (OLED), biosensor, visual light communication (VLC)

INTRODUCTION

Organic electronics is currently a nascent but rapidly growing field,[1–4] being the part of electronic science that deals with organic semiconductors (OSCs).[5] This technology provides an alternative platform for the design of low-cost, large-area, flexible, and economically viable electronic devices[6] and thus opens up new avenues of research.[7–12] It provides the complete new dimension of novel OSC-based electronic devices[5] for further realization into potential applications such as memory,[6] displays,[13] microsensors,[14–19] biosensors,[20–22] wearable fabrics,[23–27] radiofrequency identification (RFID),[28] visual light communication (VLC), and the design of novel circuits for power generation applications.[29–36] The concept is to combine the advantages of both fields, viz. organic and inorganic, to achieve far-reaching results.

OSC-based technology offers numerous advantages, including the flexible nature of such devices,[37–41] the use of unconventional substrate materials (plastics, paper, etc.),[42,43] lower fabrication costs,[44–47] etc. Flexibility[39–41] is one of the most promising benefits of this technology. Furthermore, organic technology involves low-temperature solution-based fabrication processes[48] including dip coating, screen printing,[49] inkjet printing,[50,51] etc.,

(Received December 15, 2019; accepted April 29, 2020; published online May 21, 2020)

and the utilization of unconventional substrates (fiber glass, polythene, and cloth). As a consequence, the device size is not restricted to the wafer size (a maximum of 8 inches for conventional technology), and they can be fabricated over a large area such as 10 × roll to roll.[49–51] Additionally, a huge inventory is not required[52] owing to the use of low-temperature processes.[53,54] Therefore, the overall cost of fabrication is greatly reduced.[55] Organic materials are not greatly affected by impurities,[1] hence avoiding stringent cleanroom requirements. Thus, OSC-based devices can play a vital role in future improvements to technology, providing an alternative and motivating platform to achieve low-cost consumer devices.

In comparison with conventional silicon-based technology, organic devices are superior in some regards but are lagging in others. Such devices will have far-reaching outcomes in terms of large-area fabrication,[1] flexibility,[38–41] easier manufacturing processes, robust design,[56–59] and lower cost.[50] On the other hand, in terms of characteristics such as mobility, response time, power consumption, and scaling to nanolevels, conventional silicon-based technology[1] outperforms organic devices.[51] Therefore, these two technologies can be amalgamated in the form of hybrid devices to utilize the advantages of both, as reported by various researchers.[6] Figure 1 shows a detailed comparison of organic- and inorganic-based devices (on a scale from 1 to 10), clearly revealing the advantages and disadvantages of each.

From the first report of a conducting OSC by Shirakawa et al.[60] in 1976 to the present day, substantial breakthroughs have been made. This started with the advent of thin-film technology, which revealed that materials with low mobility could also be used for the design of transistors. This led to the invention of organic thin-film transistors (OTFTs) in 1986 by Tsumuru et al.[61] However, mobility remains a significant bottleneck in the development of organic devices. Nevertheless, with rigorous research efforts, a remarkable augmentation in mobility values has been achieved. At the beginning of the 21st century, the maximum reported mobility was around 3.2 cm^2/V-s[62] for organic thin films, with an average mobility on the order of 10^{-2} cm^2/V-s or poorer. However, a value of 10 cm^2/V-s was reported by Liu et al.[63] in 2018, and average mobility values in the range from 2 cm^2/V-s to 4 cm^2/V-s were obtained. As these values remain low compared with those in conventional devices, architectural features are continuously updated to compensate for these shortcomings.

Another landmark achieved by organic devices was the successful testing of organic circuits based on OTFTs. Subsequently, the organic inverter,[6,55] as well as NAND and NOR logic gates were realized,[6,28] leading to the development of a fully organic six-transistor static random-access memory (6T-SRAM) cell[6] and other complex circuits. Other OSC-based devices such as OLEDs and solar cells have also been explored. Tang et al.[64] reported the first OLED in 1987, and thereafter, tremendous developments were reported with the passage of time. The most important practical use of OLED is in display applications for mobile phones (Apple Co.), and televisions (LG). Moreover, OLED-based sensors and VLC[65] devices have been also reported. The present review focuses on different aspects of OLEDs, focusing on the main points in their development over the years. First, the basic operating principle of an OLED is discussed, then different characteristic parameters related to OLEDs are analyzed. This is followed by a description of different methods utilized by researchers to enhance their performance.

These different methods are related to structural and material aspects, both of which are thus also reviewed comprehensively. The review of structural aspects focuses on novel structures and layers of different materials applied for performance

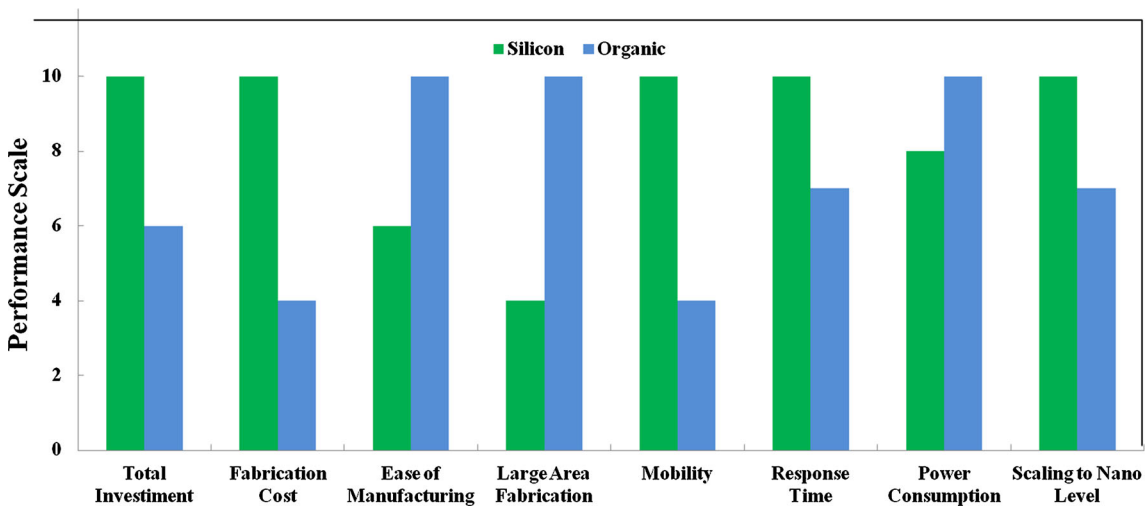

Fig. 1. Comparison of organic and conventional silicon-based technology.

enhancement. The materials summary describes the development of novel emitting materials targeting in particular the color of the emitted light. The performance of electronic devices also depends on the fabrication technology applied, thus this perspective is also given some consideration. Thereafter, models applied to provide detailed knowledge on the operation of OLED devices are considered. Different OLED applications related to the display, biomedical, and communication fields are finally explored.

This review is divided into nine sections, including the present "Introduction" section. "Organic Light-Emitting Diodes" section presents a brief summary of the operation of an OLED. Thereafter, "Characteristic Parameters" section reviews different performance parameters of OLEDs that are imperative to comprehend their specific applications. "OLED Structures" section focuses on different architectural aspects to understand the impact of the structure of an OLED on its performance. The materials facet is explored in "OLED Materials" section, whereas novel fabrication approaches are reviewed in "Fabrication Methodologies" section. "-OLED Models" *section then discusses various models developed for internal investigation of OLED structures, followed by consideration of the use of OLEDs in different novel applications in "OLED Applications" section. Finally, "Conclusions" section concludes the article with important remarks.

ORGANIC LIGHT-EMITTING DIODES

OLED device technology is growing rapidly, based on the continual evolution and development in the field of organic electronics. These devices use OSCs to generate light. Hong Kong–American physical chemist Ching W. Tang and American chemist Steven Van Slyke, at Eastman Kodak, built the first practical OLED device in 1987.[64] Since then, these devices have found wide use in display applications. The technology giants of the display arena (LG and Sony) are working on various technologies for incorporating OLEDs into their displays, with huge success. Hence, analysis of OLEDs and related techniques to enhance their performance becomes essential to stay up to date with this ever-changing technology and ensure their ongoing use.

Operating Principle

The structure of an OLED consists of an OSC material encased on two sides by electrodes. The OLED differs greatly from conventional devices, where *p*- and *n*-type sections directly connected to a supply through metal contacts are responsible for the light emission (Fig. 2a). Unlike conventional light-emitting devices, the OLED has separate electrodes for carrier injection and extraction. The structure of an OLED is illustrated in Fig. 2b. On

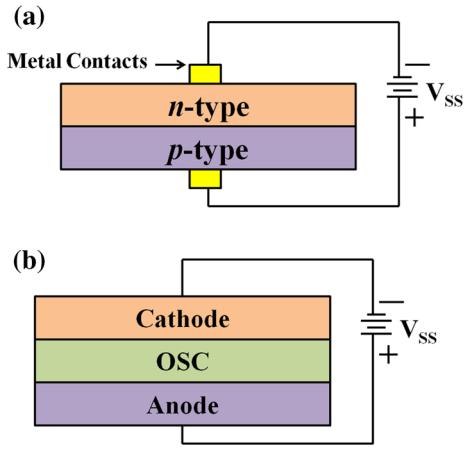

Fig. 2. Basic structure of (a) conventional LED and (b) OLED.

applying a proper bias voltage, charge carriers are injected into the device. Electrons are injected from the cathode, while holes are injected from the anode.[66] Unlike in a transistor, the electrodes are generally not interchangeable in an OLED due to its bipolar nature with different requirements for the injection of electrons and holes.

For the injection of electrons, a low-work-function electrode material such as calcium or magnesium is preferred, offering a work function that coincides with the lowest unoccupied molecular orbital (LUMO) of the OSC material. On the other hand, a high-work-function electrode material such as indium tin oxide (ITO) is required for the injection of holes. This eases the flow of holes into the highest occupied molecular orbital (HOMO) of the OSC material.[67,68] Once the charge carriers have been injected into the OSC, they start to move within the organic material, and on their recombination, energy is released in the form of light. The whole operational process of light emission from an OLED is shown in Fig. 3 and can be broadly categorized into five major steps:

(a) Injection of charge carriers
(b) Transportation of charge carriers
(c) Recombination of charge carriers
(d) Formation of excitons (i.e., excited state)
(e) Radiative decay

A brief discussion on each of these physical processes is provided below:

(a) *Injection of charge carriers:* On the application of a proper bias voltage, electrons and holes are injected into the OSC. Electrons are injected from the cathode into the LUMO, and holes from the anode into the HOMO level. The important parameter for the injection of these charge carriers is the difference in work function between the electrode and OSC the respective energy orbital[66] of the OSC. These

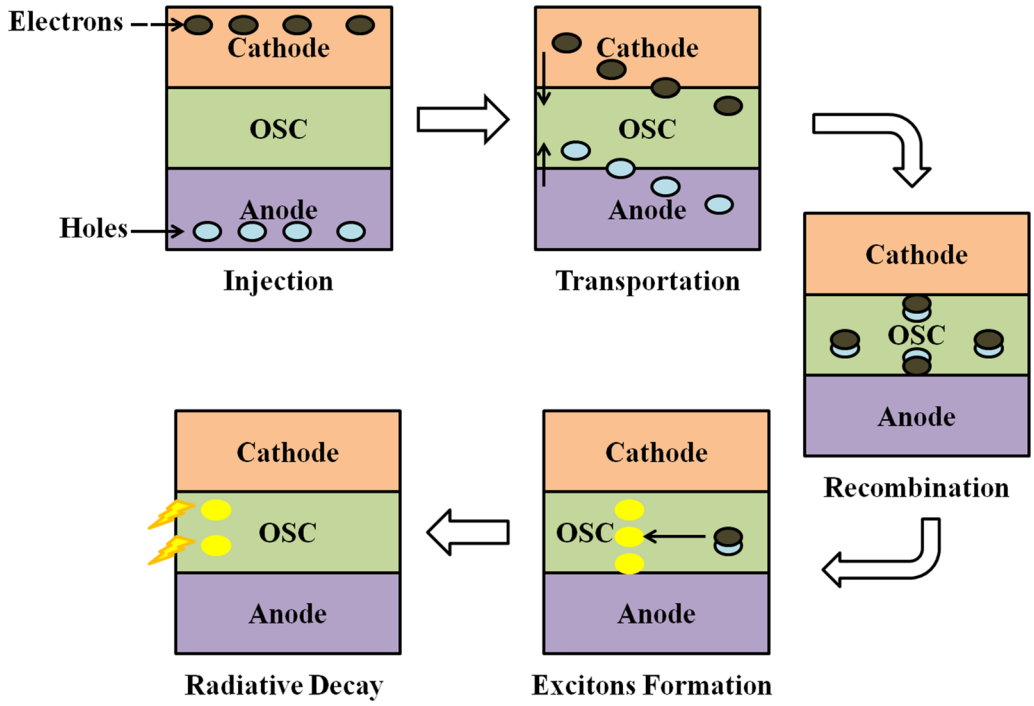

Fig. 3. Operation of OLED, depicting the series of processes for light emission.

orbitals, i.e., the HOMO and LUMO levels, are equivalent to the valence and conduction band, respectively. Generally, one of the electrodes is transparent so that light can be emitted from the device.[13] The injection can be enhanced by using specifically dedicated layers (charge injection layers) to decrease the injection barrier.

(b) *Transportation of charge carriers:* Once injected, carriers travel in the OSC to recombine with each other. However, a significant difference is observed between the mobilities of the different types of charge carrier, often being greater than two orders of magnitude.[5,28] The mobility of holes dominates over its counterpart[28,42] for all materials reported to date. This mobility difference between electrons and holes affects the recombination rate in the device. Ideally, it is desired that the recombination take place at the center of the OSC, but it actually occurs in the vicinity of one electrode due to this mobility difference.[13,66] Therefore, various architectural modifications have been suggested, mainly including the utilization of carrier transport or carrier blocking layers to address this mobility issue.

(c) *Recombination of charge carriers:* The electrons and holes move in their respective LUMO and HOMO energy levels inside the OSC. Some of these carriers come into contact with each other and recombine to form excitons, which further release energy (light) on returning to their ground state.[13] Owing to their low mobility, this recombination process in an organic semiconductor is not governed by conventional physics but can be described by Langevin theory.[69] According to this theory, the recombination rate is governed by the probability that charge carriers will find each other in such lower-mobility devices.[69] On the other hand, the recombination in conventional devices can be described by the Shockley–Read–Hall (SRH) model, specifically with faster-moving charged particles. Recombination in OLEDs may also occur by filling of trap sites. Some free carriers can also lead to the formation of excited states, thus architectural modifications also include carrier-confinement structures.

(d) *Formation of excitons:* An exciton is a state in which an electron and hole are combined because of their mutual Coulomb attraction. After recombination, the electron releases energy to return to the ground state. The energy lost by the electron is carried away by a photon in accordance with the law of conservation of energy.[66] This released energy is greatly affected by the type of semiconductor material, similar to conventional LEDs. Excitons can be of two types, viz. singlet or triplet, depending on their spin state.[66,69] Light is generated when excitons decay radiatively.

(e) *Radiative decay:* Each excited particle returns to its ground state after decaying. The decay process can be radiative or nonradiative.[66] Radiative decay results in spontaneous emission, whereas nonradiative decay leads to contact quenching and heat loss. The efficiency of fluorescent material-based devices is lower

Table I. Luminescence performance of OLEDs over the last 15 years

Year	Applied bias (V)	Luminescence (cd/m^2)	Color/Wavelength (nm)	Ref.
2004	18	10,460	Blue (492)	72
2006	20	22,350	490	73
2006	13	4067	Yellow	74
		2234	White	
2006	18	23,570	540	75
2007	25	33,000	Green	76
2007	9	16,300	525	77
2008	11.5	100	NR*	78
2010	NR	14,110	NR	79
2010	27.5	6000	NR	80
2010	NR	3000	Blue (470)	81
2011	11.5	7068	Green (tandem OLED)	82
	7.2	3133	Green (single-unit OLED)	
2012	10	63,800	Green (fluorescent)	70
	8	1,33,500	Green (phosphorescent)	
2014	16	100	408	71
2014	20	49,999	509	83
2014	10	50,000	NR	83
2018	18	45,869	Red/green (598)	85
	18	11,018	White (495–577)	
2018	NR	22,344	NR	86

than that of phosphorescent devices due to the weakness of the spin–orbital interaction that controls the intersystem crossing between the triplet and singlet states, resulting in light emission from both states. This light emission from singlet and triplet states further increases the device efficiency. As compared with a conventional LED, an OLED exhibits some unique characteristics such as (a) generation of a diverse range of colors,[66] (b) wide viewing angle,[68] (c) minimal shift in the spectral characteristics,[69] etc. Their other exclusive advantages include flexibility, low-temperature fabrication, economically viable realization, and usage of unconventional substrates. Despite all these features, advancements in OLED technology were steady, and it took almost a decade to realize potential OLED-based displays for use in practical applications.

CHARACTERISTIC PARAMETERS

There are various characteristic parameters that describe the performance of an OLED and help to ascertain its viability for a given application. The different characteristic parameters that are helpful in determining the applicability of an OLED in numerous fields include the luminescence, current density, external quantum efficiency, power efficiency, and current efficiency. Various factors affect these parameters, including the electron and hole mobility, emission material used (phosphorescence or fluorescence), device architecture, electrodes, different supporting layers, etc. Generally for an OLED, it is essentially required that these parameters should attain fairly high values.

Luminescence

The luminescence is defined as the intensity of light emitted per unit area measured in candelas per square meter (cd/m^2). It can also be described as a photometric measurement of the light traveling in a particular direction and arriving on a unit area.[69] The luminescence depends greatly on the color of light emitted, the type of material used (phosphorescent or fluorescent), the formation of excitons, the applied voltage, etc. Since good luminescence performance is a basic requirement for any OLED, a lot of effort has been investigated by the scientific community to enhance it over the last two decades. The maximum luminescence recorded for an OLED was 133,500 cd/m^2 when using 4,4′-bis(*N*-carbazolyl)-1,1′-biphenyl) doped with Ir(pyy)$_3$(fac-tris(2-phenylpyridine)iridium) dye (CBP,a phosphorescent materials) in a multilayered device structure.[70] Table I summarizes some of the best luminescence results obtained for OLEDs over the last 15 years.

The results presented in this table reveal that the luminescence has continuously improved over time, with average values in the range from 3000 cd/m^2 to 6000 cd/m^2. Different colors of light show different luminescence values, but the trend is for an increase in the luminescence for each color. The improvement in luminescence values over a period

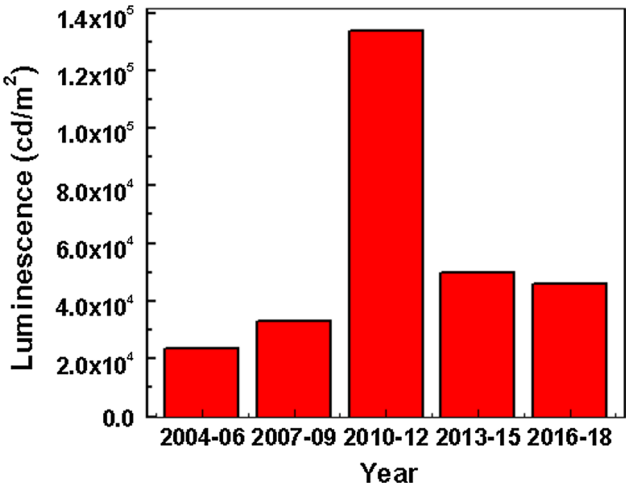

Fig. 4. Trend of luminescence over 15 years.

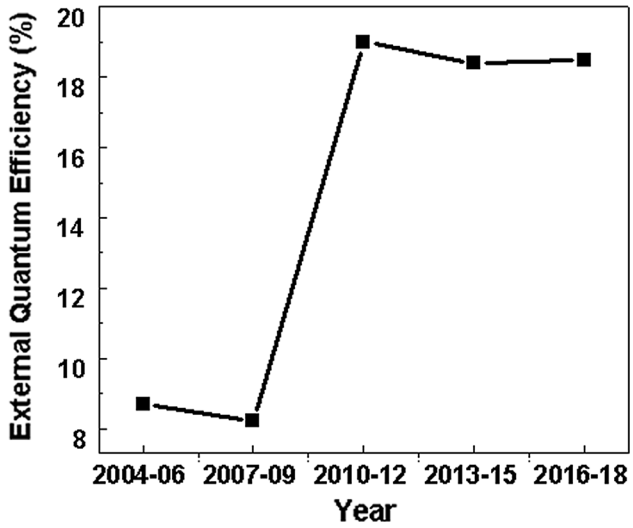

Fig. 5. Improvement in external quantum efficiency over time.

of 15 years is also illustrated in Fig. 4. Initially, Guo et al.[71] reported a low luminescence of 100 cd/m^2 for a new star-shaped material that emitted blue and ultraviolet light. Thereafter, various new approaches were applied in OLED development to enhance the luminescence characteristics. One of these included the use of double hole-blocking layers (HBLs) in the architecture.

Subsequently, Yang et al.[75] focused on the multilayered OLED architecture and improved the luminescence characteristics by 9.5% through the addition of a hole-blocking layer (HBL). Thereafter, a variety of structures such as a multilayered OLED without a HBL, and OLEDs with single and double HBLs were proposed and analyzed. Rigorous device analysis revealed that HBLs indeed help in improving the luminescence of OLEDs by directly affecting the recombination rate in the device. Through this analysis, it was observed that the luminescence could be improved from 17,000 cd/m^2 for a multilayered OLED without HBL to 23,750 cd/m^2[75] for the same OLED with the inclusion of HBLs. Similarly, Yun et al.[70] reported an improved performance for an inverted top-emitting structure with both fluorescent and phosphorescent materials. Those researchers emphasized that the thickness and proper matching of the supporting materials for the electron transport layer (ETL), hole transport layer (HTL), and HBL significantly affect the performance of the OLED. By modifying these layers, maximum luminescence values of 54,500 cd/m^2 and 133,500 cd/m^2 were achieved for fluorescent and phosphorescent materials, respectively.

Further, Ohmori et al.[76] proposed a high-performance OLED with doping of highly emissive phosphorescent dyes as host materials for emission of green and red colors. Subsequently, a device with [Ir(ppy)$_3$] showed a high luminescence of 33,000 cd/m^2, whereas a value of 8800 cd/m^2 was reported for the red-emitting dye [Ir(piq)$_3$].[76] The luminance is not high for red color, but reasonable compared with previous results.[76] Additionally, the luminescence performance of the OLED was enhanced by using a proper microcavity effect. Different researchers have shown that a Fabry–Pérot microcavity effect occurs in a multilayered OLED,[87] thereby enhancing its luminescence. Researchers including Huang et al.,[87] Zhang et al.,[88] and Chen et al.[82] worked on this and found a narrower and much brighter emission spectral width.

External Quantum Efficiency (EQE, η_{ext})

The external quantum efficiency is defined as the ratio of the number of photons emitted by the OLED to the total number of electrons passing through the device. Alternatively, it can be stated as the ratio of the number of photons emitted to the number of electrons injected into the OLED. It can be deduced from the expression

$$\eta_{ext} = n_r \times \phi_f \times \chi \times \eta_{out} = \eta_{int} \times \eta_{out}, \quad (1)$$

where η_r is the probability of electron–hole recombination to form excitons and ϕ_f is the fluorescent quantum efficiency or the fraction of excitons that decay radiatively. The probability that radiative decay occurs is represented by χ, while η_{int} is the internal quantum efficiency of the device. η_{out} represents the fraction of photons that will exit the device. According to Langevin theory for OSC materials, the EQE depends on the probability that electrons and holes will find each other. Therefore, the EQE will be higher when the concentration of electrons and holes is maximum. Figure 5 shows the improvement in the external quantum efficiency achieved over time, while Table II presents the different EQE values reported for various devices with different architectures and emission colors. This data summary reveals an increasing trend in the EQE over the years, from 2.3% in 2005 to a high value of 18.5% in 2018.[89] It should also be noted that this parameter depends greatly on the emission

Table II. External quantum efficiency (EQE) for different emission colors

Year	Applied bias (V)	Color/Wavelength (nm)	EQE (%)	Ref.
2004	18	Blue (492)	3.9	72
2005	6.1	Deep blue	2.3	91
		Sky blue	8.7	
		White		
2006	NR	NR	3.3	92
2006	13	Yellow	2.6	74
		White	1.9	
2007	9	525	1.72	77
2007	25	Green	8.2	76
2011	NR	434	1.48	93
2012	10	Green (fluorescent OLED)	2.57	70
	8	Green (phosphorescent OLED)	12.81	
2012	NR	NR	19	94
2013	NR	White (single-layered OLED)	6.7	90
		White (fluorescent OLED)	18.4	
		White (tandem OLED)	27	
		White (multilayer OLED)	14.4	
2014	16	408	2.56	71
2014	20	509	5.12	83
2014	10	NR	2	84
2018	18	Red/green (598)	5.10	85
	18	White light (495–577)	0.63	
2018	NR	Green	18.5	89

Table III. Current efficiency as function of applied bias

Year	Applied bias (V)	Current Efficiency (cd/A)	Ref.
2004	18	8.5	72
2005	6.1	12.8,16.2	91
2006	20	22.4	73
2006	18	9.16	75
2007	28	29	76
2008	11.5	2.7	78
2010	27.5	16.4	80
2011	NR	36.5	82
2012	NR	4.97	95
2013	NR	58.5	96
2014	16	10.37	71
2014	20	16.2	83
2018	15	28	97
2018	16	9.14, 10.97	85
2018	NR	59.6	89

color.[90] Green-emitting materials are most well developed and hence exhibit very high EQE values, whereas blue-emitting materials do not show such good results .

Various researchers, including Xie et al.,[89] Chang et al.,[90] and Yun et al.,[70] have reported a reasonable improvement in EQE values, including a maximum EQE of 27%, 18.5%, and 18.4% for tandem white, green, and fluorescent white light, respectively. Xie et al.[89] utilized the dip-coating fabrication technique instead of evaporation and spin coating for the realization of OLED devices. The dip-coated devices exhibited a higher EQE (18.5%) in comparison with the fully evaporated device (17.1%). Similarly, Chang et al.[90] analyzed different OLED structures based on materials emitting white light. These included a single-layer device, a fluorescent white OLED, a tandem OLED, a multiple-emissive-layer white OLED, etc. Each structure showed different external quantum efficiency. In addition, Yun et al.[70] utilized different phosphorescent and fluorescent materials to achieve high device performance. Note that the EQE is greatly affected by the choice of the material, even for the same device architecture.

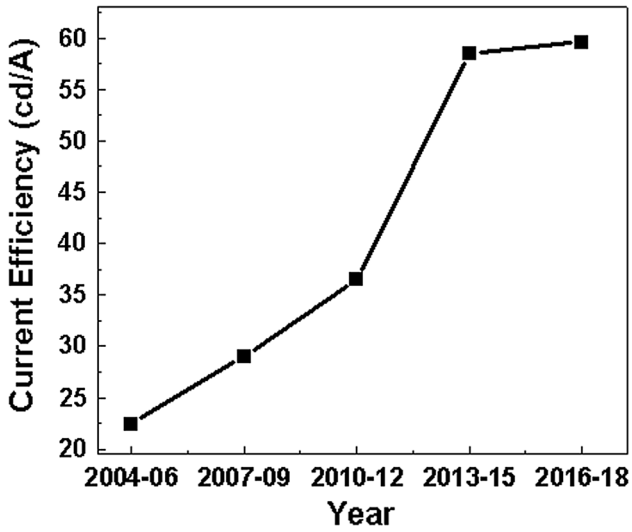

Fig. 6. Increasing trend in current density over time.

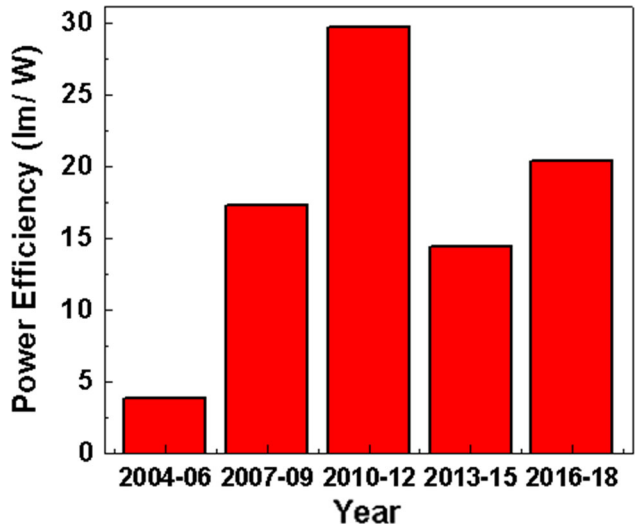

Fig. 7. Improvement in power efficiency.

Table IV. Power efficiency results for different colors

Year	Applied bias (V)	Color/Wavelength (nm)	Power efficiency (lm/W)	Ref.
2004	18	Blue (492)	3.8	72
2006	13	Yellow	2.5	74
		White	1.3	
2006	18	540	3.39	75
2007	25	Green	17.3	76
2010	NR	Blue (470)	6.53	81
2011	11.5	Green (tandem OLED)	21	82
	7.2	Green (single-unit OLED)	10.1	
2012	10	Green (fluorescent OLED)	4.6	70
	8	Green (phosphorescent OLED)	29.7	
2014	16	408	8.69	71
2014	20	460	12.9	83
		460	14.4	
2018	15	NR	20.3	97
2018	18	Red/green (598)	6.11	85
	18	White (495–577)	0.54	
2018	NR	NR	5.9	86

Current Efficiency (η_L)

Usually, the current efficiency is described as the charge transferred in a system. However, for an OLED, it is defined as the ratio of the luminescence (L) to the current density (J). This is yet another important parameter to analyze OLED performance. It is also a measure of how well the human eye can perceive a color, i.e., the photopic response of the human eye. Therefore, it also depends on the color of the light, being maximum for green light as compared with red or blue. The trend in the current efficiency also shows a continuous improvement over time, from the value of 8.5 cd/A reported by Chen et al. in 2004[72] to the maximum value of 59.6 cd/A reported by Xie et al. in 2018.[89] Table III summarizes important results for the current efficiency over the years. The increasing trend in the current efficiency over the years is plotted in Fig. 6 as well.

The most notable works reporting very high current efficiency values are as follows: Ohmori et al.[76] utilized phosphorescent material complexes of [Ir(ppy)$_3$] and [Ir(piq)$_3$] with poly(*N*-vinylcarbazole) (PVCz) and 1,3,5-tris[4-(diphenylamino)phenyl]benzene (TDAPB) as host materials for green and red light emission,[76] respectively. Using these materials, they were able to achieve a luminescence of 3800 cd/m^2 with an EQE of 8.25% and a high current efficiency of 29 cd/A. Chen et al.[82] also reported a good current efficiency of around 36.5 cd/A and a luminescence of 7068 cd/m^2[82] by using an OLED with a tandem structure. Additionally, a bulk heterojunction formed of a ZnPc and C_{60} fullerene blend was incorporated in the middle of the device. This charge generation layer

led to the formation of electrons and holes on applying an appropriate bias voltage, and transferred them to the emission layer.

Similarly, Gao et al.[96] achieved a high current efficiency of 58.5 cd/A for an OLED emitting white light via a combination of blue and yellow. They used a mixed interlayer (MI) in the device architecture. The MI provides an intermediate energy level between the two materials, thus balancing the charge carriers among them. Recently, Xie et al.[89] reported a quite high luminescence of 59.6 cd/A for a green OLED with an equally high EQE of 18.5%[89] by improving the fabrication process. OLEDs processed by dip coating show superior performance over devices fabricated by spin coating and thermal evaporation processes. Furthermore, the possibility of making large-size displays using the dip-coating process is also highlighted.

Power Efficiency (η_P)

The power efficiency is defined as the ratio of the total luminous flux (i.e., the luminous energy per unit time) to the power consumption of the OLED. It is also known as the luminous efficacy. Table IV presents the most important results for OLED power efficiencies reported in recent years, showing a steady improvement, although some of the recent data have been very low. Figure 7 illustrates the improvement in power efficiency over time. The most notable power efficiency was reported by Yun et al.[70] in 2012 for phosphorescent OLEDs. Additionally, Ohmori et al.,[76] Chen et al.,[82] Chen et al.,[83] and Li et al.[97] have also reported good power efficiency results. Ohmori et al.[76] and Chen et al.[82] worked on intermediate layers for enhancing the device performance, achieving good power efficiency values of 17.3 lm/W and 21 lm/W, respectively.

Yun et al.[70] reported an OLED based on phosphorescent materials with an inverted top architecture, including electron transportation and injection layers to enhance the device performance. The results for the device indicated a power efficiency of 29.7 lm/W,[70] in addition to a quite high luminescence of 133,500 cd/m^2. Furthermore, in 2014, Chen et al.[83] worked on novel materials such as luminogens with tetraphenylethene (TPE) to make 4-{2-[4-(Dimesitylboranyl)phenyl]-1,2-diphenylvinyl}-N,N-diphenylaniline (TPE-NB) and 4′-{2-[4′-(Dimesitylboranyl)-(1,1′-biphenyl)-4-yl]-1,2-diphenylvinyl}-N,N-diphenyl-(1,1′-biphenyl)-4-amine (TPE-PNPB) combinations. Their electron donor–acceptor interaction was found to be very strong, resulting in a decrease in the emission efficiency along with a red-shift. However, both luminogen materials showed good power efficiency of 12.9 lm/W and 14.4 lm/W for TPE-NB and TPE-PNPB, respectively.[98]

Li et al.[97] also reported a power efficiency of 20.3 lm/W for a phosphorescent blue OLED (among the highest values for blue OLEDs). In their research, two novel host materials based on C-Si and N-Si were developed. Both the silicon-containing carbazole and arysilane showed good properties, with a power efficiency of 20.3 lm/W along with an equally good current efficiency of 28.7 cd/A and EQE of 15.8% for the OLED.

Lifetime

The lifetime is another major performance parameter for OLEDs and other display devices. Even though there is no standard method for its calibration, it is measured as the mean time taken by the device to reach half its brightness.[66] The performance of OLEDs is not very good in terms of lifetime as compared with conventional LEDs. In fact, this aspect did not receive much attention from the research community, thereby hampering its improvement, but there is great scope to identify techniques that may limit the decay of organic materials over the course of time. Some of the first significant efforts aimed at increase the lifetime of OLEDs were reported by Heck et al.[99] Lifetime of less than 2000 h was reported for blue fluorescent OLEDs, which is very low compared with that of green fluorescent material, for which Weaver et al. reported a lifetime of 20,000 h.[100]

Furthermore, Wen et al.[91] analyzed blue OLED material in 2005 and reported a longest lifetime of 7000 h. The lifetime of OLEDs is affected by a number of factors, including the high device luminescence, operating specifications, and the conditions in which the devices are stored. Geffory et al.[66] also reported the lifetime of different devices depending on their emission color. Red OLEDs showed the longest lifetime of 22,000 h, followed by green at 20,000 h and blue at only 1000 h.[66] These results highlight the importance of the emission color in determining the lifetime of OLEDs. Furthermore, Tsain et al.[79] reported a short lifetime for white OLEDs. Cognizance of the heating process that occurs in OLEDs, it has been demonstrated that, with the help of heat-transmitting ultraviolet (UV)-cured glue, the device lifetime can be significantly improved.[79] Additionally, Lu et al.[81] worked on a *p*-type-doped blue OLED material, i.e., tetrafluorotetracyanoquinodimethane (F4-TCNQ) doped with {4,4′,4″-tris(*N*-(2-naphthyl)-*N*-phenylamino) triphenylamine} (2T-NATA), for the hole injection layer. Overall, the use of these materials has improved the device performance and enhanced the lifetime, reaching values as long as 3800 h.[81]

OLED STRUCTURES

OLEDs are greatly affected by the materials used in the their fabrication as well as the structure/architecture of each device. Unlike transistors, an OLED is a two-terminal diode, and architectural modifications can only be applied somewhere between the anode and cathode. However, some novel architectural modifications have resulted in

substantial performance enhancements.[101] In 1987, Tang et al.[64] first proposed a bilayer OLED consisting of two OSCs (one *p*-type and one *n*-type) between the two electrodes. However, due to the difference between the electron and hole mobility (the latter being higher in OSCs), recombination did not take place at the center where the two OSCs meet but rather inside the OSC with slower-moving charge carriers. Moreover, the high energy barrier between the electrode work function and the OSC orbital[102] is another disadvantage of this structure.

In 1995, Ammermann et al.[102] proposed a multilayered OLED architecture with each OSC layer used for a specific purpose. Charge injection was a major problem with previous structures, hence in multilayered architectures, dedicated layers are added to enhance the injection of electrons and holes. However, according to the application requirements, charge blocking layers for electrons and holes are also added to create a carrier-confinement structure so that recombination can be enhanced within the emission layer. Additionally, charge generation layers and spacer layers[73] can be incorporated into the device architecture to enhance the charge carrier concentration. To further improve the charge injection, a mixed interlayer[96] with different HOMO and LUMO levels can also be utilized. The inclusion of emission layers is also a very effective approach, where a dedicated layer is used to harness a specific luminescence.[85] Over time, novel top-emitting OLED (TOLED)[88,103] and inverted OLED architectures have also been proposed from the circuit point of view. A brief discussion of these aspects is presented below.

Additional Layers in OLED Structure

As discussed above, layers can be added to the OLED structure to enhance the injection of charge carriers. The addition of a hole transport layer (HTL)[104,105] and electron transport layer (ETL)[106] aids recombination, but the energy barrier between the electrodes and these layers makes it difficult to inject sufficient charge carriers into the device.[102] Therefore, a separate hole injection layer (HIL) and electron injection layer (EIL) are chosen for injection and transportation of charge carriers. The purpose of these layers is to reduce the barrier to injection of charge carriers by introducing an intermediate energy level between the highest occupied or lowest unoccupied molecular orbital and the work function of the electrode. Thus, a staircase-type architecture[107–110] is created, directly increasing the charge carrier injection into the OLED.[102]

Furthermore, charge blocking layers[108,109] can be introduced to restrict the movement of charge carriers. Since the hole mobility is higher than the electron mobility in organic materials, holes cross the emission layer at a higher velocity even before the electrons arrive there.[109] This results in (a) less recombination in the emission layer, (b) recombination in a layer other than the desired one, which reduces the device efficiency, and finally (c) carrier quenching at the electrodes.[110] Therefore, to restrict the movement of holes, hole blocking layers can be utilized. Once the holes are thus restricted to near the emission layer, electrons arriving at the emission layer recombine with these holes, thereby improving the device efficiency.[75] Furthermore, the assimilation of holes increases the bias of the device, which helps to inject a greater number of electrons. Table V presents the results of some of the notable work on OLED architectures.

The results presented in this table illustrate the importance of different layers in the architecture of OLEDs. The injection layer, blocking layer, along with the transportation layers[111] all have a significant impact on the performance of OLEDs; for example, adding an HIL of MoO_x improved the power efficiency by 83.7%,[86] and a similarly improvement (22%) was observed by Lu et al.[81] on using the combination of F4-TCNQ and 2T-NATA for the HIL and HTL, respectively. A spacer layer also has a considerable impact on the device performance, as observed when using LiF to separate the ETL and EML.[73] As a consequence, the luminescence efficiency of the device can be improved by sevenfold. In a similar manner, addition of other layers can enhance the characteristic performance of OLEDs. Such layers must be judiciously applied in device architectures, as they also have a direct impact on the dimensions.

Use of Novel Layers

Apart from the use of charge injection, transportation, and blocking layers to improve the performance, novel architectural modifications have also emerged for multilayered OLEDs. Some of the most promising approaches in this regard include the charge generation layer (CGL),[82] spacer layers,[73] mixed interlayer (MI),[96] microcavity structure, etc. Park et al.[112] first performed a numerical analysis on devices including a charge transport control layer (CTCL) and EML layer. It was deduced that, in the HTL/CTCL/ETL layer architecture, high HOMO and LUMO levels are preferable at the HTL/CTCL and CTCL/ETL interfaces,[112] respectively.

Chen et al.[82] made use of a charge generation layer (CGL) based on a heterojunction of ZnPc and C_{60} materials. The inclusion of these layers enhanced the charge generation and charge injection properties. The device showed enhanced performance mainly in terms of the power efficiency. In a similar manner, Gao et al.[96] used a mixed interlayer (MI) between two different emission materials. The MI can be hole or electron predominant, thus helping to balance the charge carrier transport in the device. With the help of an MI, the charge carriers could be balanced between the fluorescent blue and phosphorescent yellow materials, resulting

Table V. Layered architectures and improvement in parameters of OLEDs

Year (research group)	Device architecture	Studied layers	Analysis	Performance improvement
2004 (Chen et al.)[72]	Al (Cathode) LiF (Cathode) Alq_3 (EIL) PPOS (EML & ETL) TPD (HTL) CuPc (Buffer Layer) ITO (Anode)	1,2,3,4,5-Pentaphenyl-1-(8-phenly-1,7-octadiynyl)silole (PPOS) as EML and ETL Alq_3 as EIL and N,N′-Bis(3-methylphenyl)-N,N′-diphenylbenzidine (TPD) as HTL	Increase in thickness of TPD, Alq_3, and PPOS layer enhanced the current efficiency	1. On scaling up TPD thickness from 17 nm to 50 nm, the current efficiency increased from 1.4 cd/A to 7.7 cd/A 2. Maximum current efficiency was 8.5 cd/A when the Alq_3 thickness was 7 nm, but it decreases with decreasing Alq_3 thickness
2005 (Mori et al.)[108]	Al (Cathode) LiF (Cathode) BCP & BAlq (HBL) NPD (HTL & EML) CuPc (HIL) ITO (Anode)	Bathocuproine (BCP) Aluminum(III) bis(2-methyl-8-quinolinate)4-phenylphenolate (BAlq), both as HBL	Comparison between BCP and BAlq for better HBLs. OLED with NPD and BCP showed blue emission	1. With reduction of BAlq thickness and introduction of Alq_3, recombination zone shifted from NPD/BAlq to BAlq/Alq_3 interface 2. Electroluminescence due to BCP not observed in NPD/BCP architecture 3. Energy transfer from BCP to NPD when recombination occurs in BCP 4. BCP is a better HBL as compared with BAlq
2006 (Yang et al.)[75]	Al (Cathode) LiF (Cathode) BAlq & BPhen (HBL) Alq_3 QAD ALQ_3 (EML) NPB (HTL) m-MTDATA (HIL) ITO (Anode)	Aluminum(III) bis(2-methyl-8-quinolinate)4-phenylphenolate (BAlq) 4,7-Diphenyl-1,10-phenanthroline (BPhen), both as HBL	Compared different multilayered devices without and with single/double HBL	1. Device with double HBL showed the highest current efficiency and power efficiency 2. Current efficiency improved by 43% and power efficiency reached 3.39 lm/W, being 1.9 times higher than multilayered OLED 3. Double-HBL device also showed maximum luminescence of 23,750 cd/m^2
2006 (Kim et al.)[73]	Al (Cathode) LiF (Cathode) LiF & Alq_3 (ETL) Alq_3 (EML) NPD (HTL) CuPc (HIL) ITO (Anode)	Lithium fluoride (LiF)	Compared structures without and with LiF to separate the Alq_3 layer as EML and ETL	1. Using the LiF layer (to create a separation between the ETL and EML), the device luminescence efficiency increased by 7-fold 2. Device with LiF separation also showed highest power efficiency

Table V. continued

Year (research group)	Device architecture	Studied layers	Analysis	Performance improvement
2010 (Lu et al.)[81]	Al (Cathode) LiF (Cathode) Alq_3 & PyPySPyPy (1:1200 ratio) (ETL) TBADN & DSA-ph (EML) NPB (HTL) 3% F4-TCNQ doped 2T-NATA & 2T-NATA (HIL) ITO (Anode)	Tetrafluorotetracyanoquinodimethane (F4-TCNQ) 4,4′,4″-tris(*N*-(2-naphthyl)-*N*-phenylamino) triphenylamine (2T-NATA) TBADN{2-t-butyl-9,10-di-2-naphthylanthracene} *p*-Bis(*p*-*N*,*N*-diphenylaminostyryl) benzene (DSA-ph)	Used different combinations of F4-TCNQ and 2T-NATA as HIL and HTL	1. Bilayer of T4-TCNQ (doped with 2T-NATA) and 2T-NATA resulted in the best performance and lifetime of 3800 h, better than for undoped devices 2. Device with HIL of T4-TCNQ doped with 2T-NATA showed improved power efficiency and long operation time; it diffuses into HTL and EML and produces annihilation zones 3. Power efficiency improved by 22% in doped device
2010 (Lim et al.)[111]	Metal (Cathode) (ETL) OSC (EML) NPB (HTL) ITO (Anode)	*N*,*N*′-bis(1-naphthyl)-*N*,*N*′-diphenyl-1,1′-biphenyl-4,4′-diamine (NPB)	Variation in thickness of NPB analyzed	1. The resistance of the device and forbidden energy gap decreased with an increase in NPB thickness
2018 (Zheng et al.)[86]	Al (Cathode) LiF (Cathode) BPhen (HBL) Alq_3 (EML) NPB (HTL) MoO_x (HIL) ITO (Anode)	Molybdenum oxide (MoO_x)	Used MoO_x in solution phase as hole injection material	1. Improved device luminescence and power efficiency by 83.7% and 1.8 times, respectively, as compared with device without HIL of MoO_x 2. Compared with MoO_x deposited by other methods, solution-processed MoO_x showed best performance

in the production of white light. Previously, Park et al.[113] successfully used a spacer layer in their device architecture to separate the two different light-producing entities of the OLED.

Additional Changes in Basic OLED Structure

The basic OLED architecture suffers from many structural disadvantages,[114,115] including emission from the anode side. Owing to this, the driving circuitry can restrict the light or produce a shadow. Furthermore, the emitted light is also absorbed internally by the device. To overcome these shortcomings, some novel architectural modifications have been suggested, including an inverted OLED structure, the use of a microcavity structure, and top-emitting OLEDs. Dobbertin et al.[116] were among the first to demonstrate the fabrication of top-emitting OLEDs. The advantage of this structure is the ease of integration of the device with the driving circuitry.[66] Moreover, the circuitry does not block the emitted light, which is a common problem in OLED-based displays. The only requirement for that particular device was a transparent top electrode. Afterwards, Wu et al.,[77] Huang et al.,[114] Wang et al.,[115] and Zhang et al.,[88] also focused on top-emitting OLED structures. Table VI summarizes the work carried out by those researchers.

Table VI also highlights the importance of the microcavity effect for the luminescence characteristics of the device. Reflective anodes[88] and the ITOLED architecture[115] can be utilized to enhance the microcavity effect to improve the light output from the device. In a similar manner, the DBR effect was also used by Huang et al.[114] to improve the light output from the device; this is achieved by using multilayered electrodes. These additional architectural modifications considerably improved the device characteristics.

Microcavity Effect in OLED Structures

The OSC and electrodes used in OLEDs reflect the light. This reflected light interferes with the light emitted from the OLED, resulting in a Fabry–Pérot resonator[114] that can enhance the light output. The light output depends on the wavelength of the light and the length of the device forming the microcavity.[117,118] Choosing the correct length for the device can result in positive interference, thereby enhancing the luminescence. Researchers have successfully applied this microcavity effect to enhance the device performance. The effect is easier to use in the top-emitting OLED structure, where the bottom electrode is reflective.[119] Wu et al.[77] utilized the microcavity structure with a metallic electrode,[120] leading to a redistribution of the photon density of states (DOS), thus resulting in a certain cavity mode.[77] This led to the formation of narrow-band emission and color selection over a wide wavelength range.

Similarly, Huang et al.[114] investigated the nonzero phase shift at the interface between metallic and dielectric materials. This phase shift affects the top-emitting OLED microcavity and results in a color shift. Lee et al.[121] fabricated a resonant-cavity OLED (RCOLED) with a microcavity structure. Their work resulted in the formation of a distributed Bragg reflector (DBR) with SiO_2 and TiO_2, along with highly reflective Al metal. The results showed four emission peaks at 428 nm, 472 nm, 540 nm, and 612 nm, corresponding to deep-blue, blue, green, and red light, respectively, for white-light generation. The RCOLED exhibited enhanced luminescence, efficiency, color rendering index (CRI), and Commission internationale de l'éclairage (CIE) coordinates due to the better microcavity effect when using the optimal microcavity length. Furthermore, Huh et al.[122] used capping layers (CL) to enhance the microcavity effect in the OLED. In a bottom-emitting OLED, the CL layers helped to create a constructive interference effect, whereas in a top-emitting OLED, the CL affected the transmittance of the device.

Chen et al.[82] included a charge generation layer in a tandem OLED structure, resulting in the microcavity effect. Owing to this effect, the spectral deviation in the viewing angle was observed to be negligible. Zhang et al.[88] used Cu as a reflective anode in a top-emitting OLED, which caused a poor microcavity effect due to the lower reflectance of Cu. This resulted in lower device efficiency. Following a similar methodology, both Huang et al.[114] and Wang et al.[115] tried to modify the microcavity structure in their respective OLEDs. Wang et al.[115] utilized an inverted top-emitting OLED to include the microcavity effect, and Huang et al.[114] used stepped doping in the emission layer to fix the wavelength of the emitted light and narrow the spectral width. Both structures exhibited enhanced light output.

OLED MATERIALS

The performance of organic devices depends on the OSC material employed. In the preceding section, it was observed that different layers can be used to enhance the performance of OLEDs. In addition, different materials show different properties when applied in a particular architecture. Thus, different materials have been investigated for the emission layers. The use of different materials affects the performance of OLEDs due to their inherent properties. The organic materials along with the architecture can be combined to achieve superior devices. This section covers different materials that are used as the emission layers to output different colors of light.

Blue-Emitting Materials

OLEDs based on OSC materials have attracted much attention from researchers due to their

Table VI. Novel OLED architectures and performance improvements

Year (research group)	Structure	Analysis	Performance
2007 (Wu et al.)[77]	Ag (Cathode) Al (Cathode) LiF (Cathode) Alq_3 (EML & ETL) NPB (HTL) m-MTDATA (HIL) Ag (Anode) SiO_2 (Substrate)	Demonstrated optical and electrical properties of top-emitting OLED while varying the thickness of the Ag anode	1. Electroluminescence and reflectivity of the device with thicker anode (device 1) was higher than that with thinner anode (device 2) 2. At 7 V, the luminescence of device 1 was reported as 4078 cd/m^2 compared with 2356 cd/m^2 for device 2 3. Current efficiency of device 1 was also higher as compared with device 2: 5.2 cd/A and 2.7 cd/A respectively
2008 (Huang et al.)[114]	Ag (Cathode) Al (Cathode) LiF (Cathode) Alq_3 (EML & ETL) NPB (HTL) m-MTDATA (HIL) Au (Anode) Ni (Anode) Al (Anode) Glass (Substrate)	Analyzed the effect of multilayer anode (Ni–Au) phase shift on the performance of OLED	1. Anode exhibited periodic Ni-Au behavior similar to distributed Bragg reflector (DBR) 2. Due to presence of multicavity, there was a phase shift at the interface of metals 3. Phase shift effect altered the optical thickness of the OLED, which increased with an increase in Ni-Au pairs
2010 (Wang et al.)[115]	Alq_3 (Capping layer) Ag (Anode) MoO_3 (HIL) NPB (HTL) Alq_3 (EML) BCP (Spacer) Alq_3 (ETL) Ag (Bottom Cathode) LiF (Bottom Cathode) Al (Bottom Cathode)	Illustrated the inverted top-emitting OLED (ITOLED) structure. Anode used as the emitting electrode, and cathode as reflective electrode	1. ITOLED structure has the advantage of strong microcavity effect 2. BCP used as hole and exciton confining layer, thus improving device efficiency 3. Alq_3 capping layer on Ag anode improved the outcoupling efficiency and emission enhancement factor G_{cav} 4. Improved G_{cav} also resulted in high current efficiency and light emission intensity
2011 (Zhang et al.)[88]	Ag (Cathode) Al (Cathode) LiF (Cathode) Alq_3 (EML & ETL) NPB (HTL) MoO_x (HIL) Cu (Reflective Anode) Glass (Substrate)	Cu and MoO_x utilized as reflective anode and HIL, respectively, for top-emitting OLED	1. Device with Cu/MoO_x had enhanced luminous efficiency of 3.6 cd/A compared with 0.11 cd/A for devices without Cu/MoO_x 2. Cu/MoO_x enhanced the work function, which reduced the injection barrier for holes 3. Cu/MoO_x devices showed wide emission spectra with full-width at half-maximum (FWHM) of about 100 nm
2012 (Yun et al.)[70]	ZnS (Anode) Ag (Anode) WO_3 (Anode) NPB (HTL) Alq_3 (for Phosphorescence) & $Ir(ppy)_3$ doped CBP (for Fluorescence) (EML) Alq_3 & BPhen (ETL) CS_2Co_3 (EIL) Al (Cathode) Glass (Substrate)	Examined the effect of ETL on performance of inverted top-emitting OLED Effect of dielectric–metal–dielectric anode structure also investigated	1. Charge injection is dependent on the mobility of the ETL (even for materials with same LUMO levels) 2. The dielectric–metal–dielectric electrode resulted in low reflectance at organic–electrode interface 3. This structure subdued the strong cavity effect, but it was high enough to yield resonance-induced enhancement in luminescence efficiency

capability to produce a wide range of colors. Primarily red, green, and blue light are required for display applications.[123,124] Among these, red- and green-emitting materials are readily available and show good luminescence characteristics; however, blue-emitting materials are not on a par with these.[125] Table VII presents a comprehensive literature survey with regard to the development of blue-emitting OLED materials.

Researchers including Shi et al.,[126] Culligan et al.,[127] Hosokawa et al.,[128] and Shen et al.[129] have experimented with diarylanthracenes, but none have achieved a high-performance blue-emitting material comparable to MADN. Hosokawa et al.[128] reported on the di(styryl)arylene group based on DPVBi, which showed satisfactory performance. Wen et al.[91] further improved the structure of DPVBi to DPVPA to achieve a good-performing blue-emitting material. Wen et al.[91] utilized material engineering techniques to shorten the conjugate length of di(styryl)benzene-based dopant to a monostyrylbenzene core. Moreover, their group demonstrated that hole-blocking layers can be utilized to achieve deep-blue emission, as these layers reduce the recombination zone, consequently resulting in enhanced device efficiency.[130] Triboni et al.,[124] Suzuki et al.,[131] Luo et al.,[132] and Li et al.[97] are other researchers who have contributed significantly to the development of blue-emitting materials.

Red/Orange-Emitting Materials

The preceding section covered different research and development efforts to identify better blue-emitting materials. There are two main reasons for focusing on blue-emitting materials: their poor luminescence characteristics, and the lack of technology for their development. However, the same is not true for materials emitting green and red colors. Furthermore, a complete color display requires good red, green, and blue (RGB) color emissions. The material technology for red and green colors is quite mature, thus materials emitting in the red have not received much attention in recent times. The typical lifetime reported for red-color phosphorescent materials is 22,000 h at a luminescence of 500 cd/m^2.[99] A few details regarding red- and orange-emitting materials are presented in Table VIII.

Yellow-Emitting Materials

The basic colors that the human eye can perceive are red, green, and blue (RGB). It is the combination of these colors that creates other colors. This is also true for display devices, although there are some instances where white light is produced by some other method. The first approach in this regard is the mixing of wide-band yellow- and blue-emitting materials to produce white light.[137–139] Choukri et al.[74] produced white light by varying the position of the yellow emission of rubrene. Consequently, yellow light with CIE coordinates of (0.51, 0.48) was achieved with an external quantum efficiency of 1.3%.[74] By varying the position and thickness of the rubrene layer[140] in NPB and DPVBi, blue–yellow emission occurred, resulting in the formation of bright white light. These types of structure were previously used by other researchers including D'Andrade et al.,[141] Li et al.,[140] and Thompson et al.[142] for the generation of white light.

Akimoto et al.[137] suggested the use of benzodithiophene and triphenylamine copolymers, i.e., P-PBTx, for wide-band yellow and blue emission. Blue emission from the same material was also reported by Nishida et al.[143] According to Akimoto et al.,[137] the monomer of PhBTx exhibited white-light emission consisting of wide yellow and blue bands. They attributed the emission of yellow light to a modified molecular group such as a dimer or excimer formed between BDT moieties. Gao et al.[96] focused on the fabrication of white-light OLEDs by mixing blue and yellow light. A mixed interlayer (MI) was utilized to separate the blue-emitting material 4,4′-bis(9-ethyl-3-carbazovinylene)-1,1′-biphenyl (BCzVBi) and the phosphorescent yellow-emitting material iridium(III) bis(4-phenylthiophene[3,2-*c*]pyridibato-*N*,$C^{2'}$) acetylacetonate (PO-01). This F–I–P–I–F structure, i.e., fluorescent and phosphorescent materials separated by interlayers, was first suggested by Sun et al.[144] Other researchers including Seo et al.[145,146] and Chen et al.[135] also advocated the use of these types of structure.

Green-Emitting Materials

The human eye is most sensitive to green colors, which is why green LEDs were among the first to be developed. Furthermore, the best luminescence performance (133,500 cd/m^2) has also been achieved for green color by utilizing phosphorescent materials. The development of organic green-emitting materials started early and is now in a mature phase. Presently, most research is focused either on circuit applications,[147] or structural methods or the use of supporting materials to improve their performance. However, some novel research related to the development of green OSC materials is continuously progressing, as shown by the brief review presented in Table IX.

Alq_3 and dimethylsulfoxide (DMSO) are among the materials that show the highest luminescence performance for green light. Therefore, researchers have utilized these materials to enhance device performance. Among these, Li et al.[149] and Yim et al.[80] reported good OLED performance. Yim et al. used a poly(3,4-ethylenedioxythiophene):polystyrene sulfonate (PEDOT:PSS)[150–152] anode along with DMSO to obtain a high luminescence value of 6000 cd/m^2. Researchers including Tong et al.[153] and Krujatz et al.[125] have shown that a high EQE of 86% can be achieved with the help of fluorescent dyes. Using these fluorescent dyes, Ohomori et al.[76] reported a high luminescence of 33,000 cd/m^2.

Table VII. Different materials for development of blue-emitting OLEDs

Year (research group)	Material used	Device architecture	Performance parameters	Ref.
2004 (Chen et al.)	1,2,3,4,5-Pentaphenyl-1-(8-phenyl-1,7-octadiynyl) silole (PPOS)	Al (Cathode) LiF (Cathode) Alq_3 (EIL) PPOS (EML & ETL) TPD (HTL) CuPc (Buffer Layer) ITO (Anode)	1. PPOS emitted blue light at 492 nm 2. Highest values of parameters Luminescence—10,460 cd/m^2 Current efficiency—8.5 cd/A External quantum efficiency—3.9% Power efficiency—3.8 lm/W	72
2005 (Wen et al.)	Diarylanthracene group: 2-Methyl-9,10-di(2-napthyl)anthraxcene (MADN) 2-(*t*-Butyl)-9,10-di(2-napthyl)anthraxcene (TBADN)	Al (Cathode) LiF (Cathode) Alq (ETL) MADN (EML) NPB (HTL) CF_x (HIL) ITO (Anode)	1. Both materials show potential for deep-blue OLED application 2. MADN exhibits current efficiency of 1.4 cd/A with CIE of (0.15, 0.10) for blue light 3. TBADN has CIE of (0.13, 0.19), but its efficiency was poor	91
	Di(styryl)arylene group: DPVA (replacing central biphenyl nucleus of DPVBi with diphenyl anthracene).	Al (Cathode) LiF (Cathode) Alq (ETL) TBD doped MADN (EML) NPB (HTL) CF_x (HIL) ITO (Anode)	1. DPVPA has higher quantum efficiency than DPVBi 2. It shows fluorescence of 448 nm with 20 nm green shift 3. External quantum efficiency is 3% more than MADN with CIE of (0.14, 0.17), i.e., slightly greener	
	Tetra(*t*-butyl) perylene (TBP) group: TBD doped in MADN (0.5% v/v)	Al (Cathode) LiF (Cathode) Alq (ETL) TBD doped MADN (EML) NPB (HTL) CF_x (HIL) ITO (Anode)	1. Current efficiency of 3.4 cd/A with CIE of (0.13, 0.20), representing sky-blue color 2. The material did not have functional group, therefore its emission properties cannot be altered	
	Diphenylamino-di(s-tyryl)arylene (DSA-ph) group: Bis(diphenyl)aminostyryl benzene (DSA-ph)	Al (Cathode) LiF (Cathode) Alq (ETL) DSA-Ph doped MADN (or DPVPA) (EML) NPB (HTL) CF_x (HIL) ITO (Anode)	1. Absorption at 410 nm with fluorescence at 458 nm 2. When 3% DSA-ph is doped with MADN, the observed current and power efficiency are 9.7 cd/A and 5.5 lm/W, respectively 3. Expected lifetime of 46,000 h	
2006 (Fischer et al.)	*N*,*N*′-Diethyl-3,3′-bicarbazyl (DEC) 4,4′-bis(2,2′-diphenylvinyl)-1,1′-biphenyl (DPVBi)	Al (Cathode) LiF (Cathode) Alq_3 (ETL) BCP (HBL) DEC & DPVBi (EML) NPB (HTL) CuPc (HIL) ITO (Anode)	1. 2% DEC doped in DPVBi 2. The device shows EQE, current efficiency, and power efficiency of 3.3%, 4.7 cd/A, and 1.3 lm/W with luminescence of 2825 cd/m^2 3. Good deep-blue emission	92

Table VII. continued

Year (research group)	Material used	Device architecture	Performance parameters	Ref.
2011 (Lee et al.)	4-Hydroxy-8-methyl-1,5-naphthyrdine aluminum chelate ($AlmND_3$)	Al (Cathode) LiF (Cathode) $AlmND_3$ (EML) mCP (Buffer Layer) NPB (HTL) ITO (Anode)	1. Material showed ambipolar nature with electron and hole mobility of 5×10^{-5} cm^2/V-s and 1×10^{-5} cm^2/V-s, respectively 2. CIE of material is (0.16, 0.08), i.e., deep-blue emission 3. EQE of device is 1.59% with luminescence of 3730 cd/m^2	93
2014 (Guo et al.)	Star-shaped molecule (SSM) with carbazole and arylamine backbone	Al (Cathode) LiF (Cathode) TPBi (ETL) SSM doped DSA-Ph (EML) TCTA doped NPB (HTL) 2T-NATA (HIL) ITO (Anode)	1. Emission of SSM in wide range of 375 nm to 525 nm with peak at 408 nm 2. Current efficiency of 10.37 cd/A with power efficiency of 8.6 lm/W	71
2015 (Wahyuningrum et al.)	Nitrated *N*,*N*-diphenylamine (DPA)	NR	1. After nitration process, material showed absorption peaks at 337 nm and 406 nm, corresponding to peak emission of normal DPA, i.e., 330 nm 2. Emission peaks of new material at 413 nm and 498 nm, corresponding to blue emission	123
2015 (Triboni et al.)	4-(2-Fenoxi-*p*-xileno) *N*-methyl-1,8-naphthalimide (NPOX)	Al (Cathode) NPOX (EML) PEDOT:PSS ITO (Anode)	1. Emission spectrum of NPOX centered at 435 nm with mobility of 5×10^{-5} cm^2/V-s 2. Reported CIE is (0.211, 0.313), corresponding to blue emission	124
2016 (Krujatz et al.)	2′-7′-Di-*tert*-butyl *N*,*N*-diphenyl-7-(4-(1-phenyl-1*H*-benzo[*d*]imidazole-2-yl)phenyl)-9,9′-spirobi[fluorene]-2-amine (spiro-bifluorene derivatives)	Al (Cathode) Ba (Cathode) TPBi (ETL) Spirobifluorene Derivative PEDOT ITO (Anode)	1. Material emitted blue light at 457 nm 2. EQE of 2.9% with maximum luminescence of 1717 cd/m^2 3. Reported CIE is (0.17, 0.10)	125
2018 (Li et al.)	3,9-Bis(triphenylsilyl)-9*H*-carbazole (SiCzSi) 3,6,9-Tris(triphenylsilyl)-9*H*-carbazole (DSiCzSi)	Al (Cathode) MoO_X/ LiF HOST MoO_X/ LiF ITO (Anode)	1. DSiCzSi has current and power efficiency of 25 cd/A and 16.4 lm/W, respectively, with EQE of 13.7% 2. SiCzSi showed current efficiency of 28.7 cd/A along with power efficiency of 20.3 lm/W. EQE reported to be 15.8%	97

Table VIII. Device architecture and performance for red/orange-emitting materials

Year (research group)	Material	Device Architecture	Reported Results	Ref.
1989 (Tang et al.)	4-(Dicyanomethylene)-2-methyl-6-(*p*-dimethylaminostyryl)-4*H*-pyran (DCM)-doped Alq_3	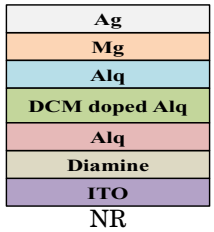	1. Emission wavelength observed between 610 nm and 650 nm, corresponding to orange and red color	133
2006 (Ko et al.)	4-(Dicyanomethylene)-2-*t*-butyl-6(1,1,7,7-tetramethyljulolidyl-9-enyl)-4*H*-pyran (DCJTB) and rubrene-doped Alq_3	NR	1. CIE for both materials was (0.64, 0.36) 2. Current efficiencies—2.5 cd/A and 3.2 cd/A 3. Power efficiencies—0.9 lm/W and 1.2 lm/W	134
2007 (Ohmori et al.)	Tris-(1-phenylisoquinoline)iridium [$Ir(piq)_3$]-doped PVCz–TDAPB	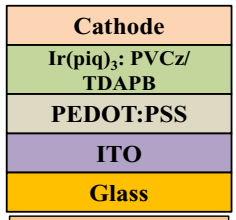	1. Reported external quantum efficiency 6.3% 2. Power efficiency 3 lm/W 3. Luminescence 6000 cd/m^2 and 820 cd/m^2 for PVCz and TDAPB devices, respectively	76
2010 (Chen et al.)	4-(Dicyanomethylene)-2-*t*-butyl-6(1,1,7,7-tetramethyljulolidyl-9-enyl)-4*H*-pyran (DCJTB)-doped MADN	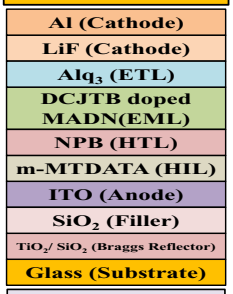	1. DCJTB emission for conventional and resonant-cavity OLED at 560 nm and 612 nm, respectively 2. Emission of red/orange light observed Luminescence efficiency—6.32 cd/A Carrier lifetime—1.53 ns	135
2012 (Huh et al.)	2,6-Bis(3-(carbazol-9-yl)phenyl) pyridine (DCzPPy) Bis(2-phenylbenzothiozolato-$N,C^{2'}$) iridium(III) (acetylacetonate) (Bt2Iracac)	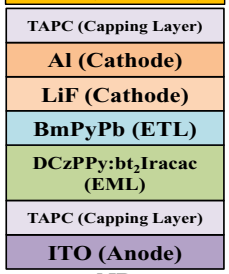	1. On the top-emitting side, the EQE increased from 1.90% to 3.06% with the use of capping layer 2. In contrast, on the bottom side, the use of capping layer decreased the EQE from 11.55% to 10.10% 3. The intensity of radiance for red light at 565 nm and 605 nm decreased till capping layer thickness of 60 nm, increasing thereafter	122
2015 (Kim et al.)	Quantum dots (QDs)	NR	1. Quantum dots used to enhance the emission intensity for the red color along with absorption of unwanted green and blue light	136
2018 (Zhou et al.)	4-(Dicyanomethylene)-2-*t*-butyl-6(1,1,7,7-tetramethyljulolidyl-9-enyl)-4*H*-pyran (DCJTB)-doped Alq_3	Mixed device architecture to emit white light	1. Device showed Maximum luminescence of 45,869 cd/m^2 Current power of 9.14 cd/A Power efficiency of 6.11 lm/W EQE of 5.10% 2. Electroluminescence varied from 644 nm to 598 nm, resulting in red to red–green emission	85

Table IX. Reported work on development of green-emitting materials for OLEDs

Year (research group)	Material	Device structure	Performance	Ref.
1997 (Shi et al.)	5,12-Dihydro-5,12-dimethylquino[2,3-*b*]acridine-7,14-dione (DMQA)-doped Alq_3	Ag (Cathode) Mg (Cathode) Alq (ETL) Alq_3: DMQA (EML) NPB (HTL) CuPc (HIL) ITO (Anode)	1. Reported CIE of device is (0.39, 0.59) 2. Current efficiency is reported as 7.3 cd/A	148
1997 (Jabbour et al.)	*N*,*N*′-diphenylquinacridone (QAD)-doped Alq_3	AL (Cathode) LiF (Cathode) Alq_3: QAD (EML) TPD (HTL) ITO (Anode) Glass (Substrate)	1. Insertion of Mg into the Al electrode to improve the characteristics 2. EQE is observed to increase from 3% to 3.2% with use of Mg	5
2006 (Li et al.)	Tris(8-hydroxyquinoline) aluminum (Alq_3)	Al (Cathode) LiF (Cathode) BCP (HBL) Alq_3 (EML & ETL) TPD/ NPB (HTL) PVK (CBL) PEDOT:PSS (HIL) ITO (Anode) Glass (Substrate)	1. Alq_3 device emission is in green range with peak at 520 nm and full-width at half-maximum (FWHM) at 90 nm 2. Introduction of the hole blocking layer increased the device luminescence twofold	149
2007 (Ohmori et al.)	Fac-tris(2-phenylpyridine) iridium ($Ir(ppy)_3$)-doped 1,3,5-tris[4-(diphenylamino)phenyl] benzene (TDAPB)	Cathode $Ir(ppy)_3$ doped TDAPB (EML) PEDOT:PSS (HTL) ITO (Anode) Glass (Substrate)	1. The device exhibited External quantum efficiency—8.2% Power efficiency—17.3 lm/W Maximum luminescence—33,000 cd/m^2	76
2010 (Yim et al.)	Dimethylsulfoxide (DMSO)-doped PEDOT:PSS as anode and $Ir(ppy)_3$-doped TPD as emission layer	Al (Cathode) LiF (Cathode) $Ir(ppy)_3$:TPD(EM) DMSO:PEDOT:PSS (Anode) PES (Substrate)	1. Device showed low turn-on voltage of 4.5 V 2. Highest luminescence—6000 cd/m^2 (Bias voltage—27.5 V) 3. Maximum current efficiency—16.4 cd/A (At 8.5 V)	80
2011 (Chen et al.)	Zinc phthalocyanine (ZnPc):fullerene (C_{60}) as CGL Alq_3 as EML	Al (Cathode) LiF (Cathode) NPB MoO_3 ZnPc:C_{60} LiF Alq_3 LiF ITO	1. The modified tandem device yielded power efficiency twice (21 lm/W) that of the conventional OLED 2. They also reported twofold improvement in luminescence and current efficiency	82

Table IX. continued

Year (research group)	Material	Device structure	Performance	Ref.
2016 (Krujatz et al.)	Bis(2,6-diphenylpyrimidinato)iridium(III) picolinate [Ir(ppm)$_2$(pic)] Bis(2,6-diphenylpyrimidinato)iridium(III) 5-(2′-pyridyl)-3-trifluoromethyl-1,2,4-triazolate [Ir(ppm)$_2$(taz)]	Ag (Cathode) Ca (Cathode) TPBi Ir(ppm)$_2$(pic) or Ir(ppm)$_2$(taz) PEDOT:PSS ITO	1. Ir(ppm)$_2$(pic): The emission wavelength was 549 nm, with EQE of 83% 2. Ir(ppm)$_2$(taz): The emission wavelength was 523 nm, with reported EQE of 86%	125

FABRICATION METHODOLOGIES

The various fabrication processes used for realizing a device play an important role in determining its performance. Even a minute error can result in complete alteration of the device performance. However, at the present time, fabrication processes are standardized to such a high precision level that yields are very high. Fabrication of a conventional transistor follows a very complex flow which includes photolithography,[154] masking,[155] thermal evaporation,[156] ion implantation and diffusion. In contrast, solution processes such as spin coating, the Langmuir–Blodgett (LB) process,[157,158] dip coating,[159] inkjet printing,[98] polymer inking, stamping,[147] transfer printing,[160] etc. are used to fabricate OLEDs. These techniques are usually employed at room temperature and thus do not require huge inventory. High-temperature processes may destroy the atomic structure of OSCs and are thus avoided.

The basic fabrication process for an OLED starts with selecting a substrate or electrode. For a conventional OLED, generally an ITO electrode is preferred, but novel electrode materials such as nontoxic aluminum-doped zinc oxide (AZO)/Ag/AZO[95] or Al have also been utilized. In case of a flexible electrode (PEDOT:PSS), glass or plastic is utilized to provide the mechanical support. The first fabrication process includes cleaning of the substrate/electrode to remove any contamination from the surface, as illustrated in the flowchart shown in Fig. 8. This includes a set of cleaning processes such as dipping in acetone and isopropanol, treatment in an ultrasonic bath, followed by oxygen plasma treatment[161] and drying using a nitrogen gun. Afterwards, the electrode is deposited by sputtering[149] (ITO), magnetic sputtering (AZO/Ag/AZO),[95,162,163] and thermal evaporation (metallic electrodes, Al or Cu). Thermal deposition techniques are carried out in a thermal evaporation chamber at high pressure.[70,164]

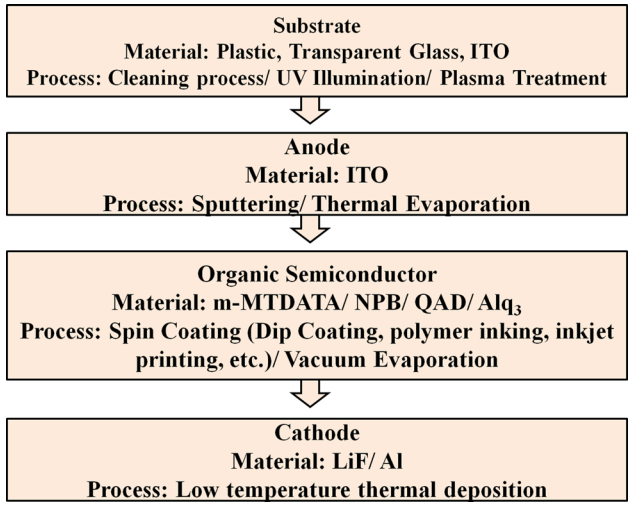

Fig. 8. Basic fabrication flow of bottom-emitting OLED.

The OSC is deposited using either thermal deposition or solution processes.[1] Thermal evaporation techniques are utilized to deposit small-molecule materials, as their structure is not affected by high temperatures[165–167] and solvents for these materials are not readily available.[1] Solution processes are employed for conducting polymers, as they dissolve easily in organic solvents. Solution processes are carried out at low temperature and are very cost effective, thereby invariably being utilized for fabrication of large-scale flexible devices and displays. Finally, the top electrode is deposited with the help of a low-temperature high-pressure thermal evaporation process that does not damage the underlying OSC layer.

To achieve OLEDs with better performance, researchers have tried to enhance and develop new fabrication processes over the last decade. Jenfeng et al.[168] deposited PEDOT nanoparticles as a hole injection layer by using the LB technique.[157] Their analysis revealed that the LB process deposited PEDOT particles with much smaller

size (20 nm to 40 nm),[168,169] thus their device showed a higher current density than that fabricated by conventional methods. Keum et al.[170] developed a blading technique[171,172] specifically for liquid-crystalline OSC[171,173,174] to adjust the molecular orientation. Along with this, an annealing process was also utilized.[170,175] When adopting these techniques, the efficiency of the device was significantly increased owing to the proper alignment of the liquid-crystal OSC molecules.

Recently, Zheng et al.[86] compared the performance of two different OLEDs based on HIL deposition using a low-cost solution process[176–178] and an evaporation process.[86] In the former case, the deposition of MoO_x (as the HIL) was performed by spin coating (at 4000 rpm for 60 s) followed by an annealing process. This device exhibited current and power efficiencies of 7.9 cd/A and 5.9 lm/W, respectively, being 43.6% and 73.5% higher than for the device fabricated using the vacuum evaporation process. Furthermore, Xie et al.[89] utilized dip coating[179–181] to deposit the transport and emission layers. By controlling the dipping time, speed, and concentration of solution, they achieved a current efficiency of 4.6 cd/A and power efficiency of 2.6 lm/W with dip-coated layers. All these results illustrate the impact of fabrication methodologies on the device performance.

OLED MODELS

Mathematical models are often used for predicting the internal device physics and understanding device operation.[182,183] This helps to analyze the device performance under different conditions.[184] Various researchers have developed the mathematical models that are essentially required to understand the physics behind carrier injection and transportation within different layers, thus leading to the innovation of novel device architectures.

Numerical Analysis Based on Poisson's Equation

Poisson's equation is among the most important equations used by mathematicians and physicists.[184] Malliaras et al.[185] applied this equation to calculate the spatial charge distribution inside an OLED and investigated the role of injecting the charge carriers along with their mobility on the device performance. The results illustrated a requirement for equal mobility for electrons and holes, which results in an enhanced recombination rate. Chan et al.[186] also adopted Poisson's equation with an additional optical model to analyze the microcavity effect and determine the optical thickness.[186]

Park et al.[112,113,187] utilized Poisson's equation along with drift–diffusion and singlet exciton rate equations to analyze the internal physics of the device.[184] Their group performed numerous numerical analyses on OLEDs based on this set of equations and investigated the temperature dependence[188] of OLEDs and their different energy loss mechanisms.[113] This analysis revealed that the loss phenomenon occurs based on the absorption of photons emitted from thin quantum wells in conventional LEDs, whereas in organic devices, this loss occurs due to energy transfer from the layer with a higher transition energy.

OLED Model Based on Atomistic Simulation

Work based on atomistic simulation was carried out by Nagata et al.[189] in 2008, wherein the electrostatic potential charges are used to calculate the site energies. Additionally, the Miller–Abraham equation is employed to calculate the charge mobility. This analysis was undertaken to better understand the Poole–Frenkel (PF) mobility model. The analysis began with Gill's law[189] followed by the Miller–Abraham-type hopping rate. Thereafter, the calculation of the mobility μ is completed with the help of Marcus theory. The results of their analysis confirmed the Poole–Frenkel-type behavior of the charge carrier mobility because of the electric field. Four key issues are addressed in their analysis:

1. The site energy distribution is much wider for an amorphous material, and it governs the PF behavior of the charge mobility;
2. The spatially correlated site energy is not the dominant mechanism underlying the PF behavior;
3. To explain the PF behavior, it is necessary to have random mesh connectivity in a three-dimensional amorphous structure;
4. The charge carrier density is dependent on the charge carrier mobility and it results in an enhancement of the PF dependence of the mobility versus the electric field in the space-charge-limited current.

Modeling of Thermal Properties of OLEDs

Bergemann et al.[94] used the transmission matrix approach to model the effect of different thermal effects such as convection, conduction, and radiation on the OLED temperature. This approach uses the Laplace transform for the heat transfer equations. The layers are treated as the product of the transmission matrices for several films (in series), whereas the incident heat flux is assumed to be fragmented between the two isolated independent channels with no flow between them (in parallel). These two channels, parallel and series, are then combined to model the heat transfer.

Numerical Analysis of OLEDs Based on Maxwell's Equations

Pflumm et al.[190,191] developed a model driven by the current for OLEDs in the context of the drift–

diffusion model. The process governing the formation of excitons is assumed to be Langevin. A method for the calculation of the electric fields based on Maxwell's equations is described. This method is helpful, as it differentiates between the current and the voltage excitation of the OLED. The current and voltage behavior of the OLEDs can be modeled using both methods, although the method is much quicker when the current is specified.

The above-mentioned models completely predict the thermal profile of the OLED accurately, thus providing an understanding of the various factors that determine the device operating temperature. Such models can also be utilized for numerical analysis of OLEDs consisting of different layers, viz. emission layers and charge transport control layers (CTCL), similar to the work of Park et al.[112] Moreover, these affect the analysis of the energy loss mechanisms in different device structures, thereby enhancing the architectural aspects.

OLED APPLICATIONS

Currently, OLEDs are at the apogee of OSC-based display technology. These devices offer numerous advantages which can be used in a range of applications. The most well-known applications of OLEDs include display and sensor technology. There are some reported cases of use of OLEDs in VLC links as well. These main applications of OLEDs are reviewed in this section.

OLED-Based Displays

Displays are one of the major applications based on OLEDs and have seen considerable improvement over the past decade. Technology giants such as LG and Apple are incorporating OLED-based displays into their devices. The main reason for this shifting trend from inorganic LEDs to OLED is the impeccable color properties and contrast that OLED-based displays offer. OLED displays are also better in that they do not require any backlighting,[1] resulting in better contrast. Further, they can generate a wide variety of colors, resulting in enhanced image output. Present research is focused on enhancing their efficiency, as the OLED is the component that consumes most power in any circuit. Shin et al.[192] employed dynamic voltage scaling, as there is no particular power saving methodology which incorporates a minimum change in OLED color. The proposed method suggests scaling down the voltage supply, which results in a reduced power requirement due to the lower voltage drop across the driver transistor. The overall power saving is reported to be 52.5% in comparison with other methods.[192]

Similarly, Wee et al.[193] adopted a method known as saliency to reduce the power consumption of OLEDs. The method depends upon the amount that a particular image stands out from a particular scene. The power is reduced in areas which are not in direct eye contact. The overall approach, first used by El-Nasr et al.,[194] is to differentiate between areas of direct and indirect focus. The approach saved 11% of the display power and 4% of the device power.[193] Further, Lin et al.[195] enhanced the technique for scaling of image pixels. By scaling down the pixel values, it gives the user flexibility to scale even irregular shapes. In their method (CURA), saliency was also incorporated. Any type of display device is swept continuously by refresh current signals numerous times during operation. These signals cause a lot of stress on the OLED and result in shorter lifetime and poor performance. In this regard, Liu et al.[196] analyzed the impact of different types of applied voltages on OLED performance.

This is a follow-up of the work proposed by Jacobs et al.[197] and Buso et al.[198] In their work, it was observed that the amplitude modulation technique for direct current (DC) can help to dim an OLED effectively, as long as multiple emitters are not involved. Lin et al.[199] proposed a new buck driver for OLEDs, as the dimming response of the device is strongly influenced by its own heavy parasitic capacitance. The buck driver circuitry also includes a variable-frequency control mechanism. This resulted in a reduction of the output voltage rise time from 25 μs to 10 μs with a corresponding reduction in the switching frequency from 100 kHz to 48 kHz. In a more recent article, Fan et al.,[200] presented an active-matrix (AM)OLED display driven by polysilicon TFTs. A high display operating speed can be achieved using the presented scheme. It was observed that the OLED display has a high frame rate of 240 kHz for an emission driving scheme and the input data period must be 3.5 μs.

OLEDs as Sensors

Sensing is another potential application of OLED-based devices. Various researchers are working on light-based detection, as almost every element in the Periodic Table interacts with light. These particles absorb a light of a particular wavelength to reach a higher excited state, then release this energy when returning to the ground state.[201] The wavelength of the light absorbed by a particular element is fixed (based on its bandgap). Furthermore, OLEDs are known to emit a wide range of colors, implying that light with two colors of similar wavelengths can easily be differentiated. This property can be precisely controlled and is therefore used to differentiate between various elements more accurately.

Miyamoto et al.[202] utilized OLED-based displays for chemical image sensing. The sensor is based on the principle of a light addressable potentiometric sensor (LAPS). Werner et al.[203] further worked on an OLED-based LAPS sensor with a much better response time. The driving methodology suggested by them resulted in modulation frequencies in the

range from 1 kHz to 16 kHz, which directly enhanced the sensing speed by 40 times compared with previously reported devices. Thereafter, many research articles reported the use of OLEDs as photoluminescence sensors, biosensors, and absorption and transmission sensors.[99] Shinar et al.[204] described gas sensors based on the photoluminescence properties of OLEDs. Their method used Ru complexes that are sensitive to oxygen, thus the luminescence intensity of the OLEDs becomes dependent upon the oxygen concentration.

The advantage of using OLEDs in sensor applications is that they provide a noninvasive method.[125,205] Sensors based on the emission from OLEDs with organic photodiodes (OPDs) for detection have also been reported.[206] These sensors can be tuned to become sensitive to different elements or compounds such as oxygen, ammonia, or carbon dioxide. A novel approach in this regard suggests the replacement of the OPD with an OLED for the detection of the light[201] as well. The OLED can thus be utilized as both the light source and detector for primary screening of ovarian cancer.[201] Temperature can also be sensed[205] utilizing OLEDs.

Krujats et al.[125] used the DBR effect to control the light emission from a top-emitting OLED. Based on the excitons from the OLED and the emission of light from the particles to be detected, OLED-based sensors can be utilized in many different ways. Only a small number of biosensors using the transmission and scattering effect have been reported. Prabowo et al.[207] detected anti-mouse immunoglobulin G with the help of an OLED integrated with a surface plasmon resonance device. Biocatalysis is another approach in which the photoluminescence of OLEDs can act on co-embedded enzymes or catalysts. Choudhury et al.[208] presented this approach for a glucose biosensor based on oxygen-sensitive dyes such as Ru or Pt along with glucose oxidase (GOx) in a solution gel sensor film.

OLEDs in VLC Devices

VLC relies on sending information in the form of light due to its highest speed. OLEDs can be used as sources for such devices. Unfortunately, work regarding the use of OLEDs as light sources for VLC is not widely reported. To date, the VLC field has been dominated by conventional LEDs, as they offer high optical power and wide bandwidth.[209] However, at the same time, being a point source, these devices may be harmful and can cause damage to human eyes.[65] Therefore, OLEDs are much more suitable for this particular application owing to their low cost and flexible nature.

Haigh et al.[210,211] first reported an OLED-based VLC device, wherein OLEDs and photodetectors were utilized to create a 1.4-Mbps link using discrete multitone modulation. Their group also analyzed pulse modulation schemes including pulse position modulation (PPM) and on–off keying (OOK). Their analysis revealed that, when using the OOK modulation scheme, OLED-based VLC was limited to a data rate of 550 kbps. Thereafter, their work supported the use of the PPM scheme with the inclusion of an improved driving scheme. After this, equalization of the signals was also performed, resulting in a VLC link with speed of 2.7 Mbps,[65] representing a twofold improvement in speed compared with another defined scheme.

CONCLUSIONS

This exhaustive review covers various aspects of OLEDs, such as performance parameters, device architectures, different materials, fabrication techniques, and applications. Scientific and research advancements related to these aspects over the past two decades are covered in depth, and their impact on OLED performance discussed. A number of challenges have been addressed, and researchers have made continuous progress towards successful commercialization of OLEDs. These include enhancement of the device architecture, which is instrumental for improving their performance characteristics. The development of novel materials has also played an important role in achieving excellent luminescent characteristics. Display-based applications have already been developed and show huge commercial potential.

There are still numerous aspects that could be improved and should become research focuses in the near future. These include the development of application-specific OLED materials with a focus on novel sensors and VLC devices. Material properties should also be improved, bearing in mind the domain-specific requirements. Further, the lifetime of the developed materials and devices should become a center of focus. In this regard, device packaging methodologies should be improved to prevent degradation of OLEDs under various atmospheric conditions. This will lead to greatly improved and enhanced lifetimes. OLEDs are multifaceted devices, so additional novel, contemporary, state-of-the-art applications should be investigated. These may lie in the fields of sensors and VLC devices. Novel sensors could be developed to act as both the light source and detector, as well. Additionally, organic devices should be complemented with silicon-based devices. This will lead to a boost in the present technology with a focus on combining the advantages of both approaches, which may result in highly superior devices.

REFERENCES

1. B. Kumar, B.K. Kaushik, and Y.S. Negi, *Polym. Rev.* 54, 33 (2014).
2. X. Fan, J. Chen, J. Yang, P. Bai, Z. Li, and Z.L. Wang, *ACS Nano* 9, 4236 (2015).
3. J. Yang, J. Chen, Y. Liu, W. Yang, Y. Su, and Z.L. Wang, *ACS Nano* 8, 2649 (2014).

4. Z. Lin, J. Chen, and J. Yang, *J. Nanomater.* 2016, 5651613 (2016).
5. G.E. Jabbour, Y. Kawabe, S.E. Shaheen, J.F. Wang, M.M. Morrell, B. Kippelen, and N. Peyghambarian, *Appl. Phys. Lett.* 71, 1762 (1997).
6. B. Kumar, B.K. Kaushik, and Y.S. Negi, *Microelectron. Reliab.* 54, 2801 (2014).
7. J. Chen, G. Zhu, J. Yang, Q. Jing, P. Bai, W. Yang, X. Qi, Y. Su, and Z.L. Wang, *ACS Nano* 9, 105 (2015).
8. W. Yang, J. Chen, X. Wen, Q. Jing, J. Yang, Y. Su, G. Zhu, W. Wu, and Z.L. Wang, *ACS Appl. Mater. Interfaces* 6, 7479 (2014).
9. X. Zheng, B. Chen, C. Wu, and S. Priya, *Nano Energy* 17, 269 (2015).
10. Y. Wu, Q. Jing, J. Chen, P. Bai, J. Bai, G. Zhu, Y. Su, and Z.L. Wang, *Adv. Funct. Mater.* 25, 2166 (2015).
11. C. Yan, Y. Gao, S. Zhao, S. Zhang, Y. Zhou, W. Deng, Z. Li, G. Jiang, L. Jin, G. Tian, and T. Yang, *Nano Energy* 67, 104235 (2020).
12. G. Zhu, B. Peng, J. Chen, Q. Jing, and Z.L. Wang, *Nano Energy* 14, 126 (2015).
13. A. Dodabalapur, *Solid State Commun.* 102, 259 (1997).
14. J. Chen and Z.L. Wang, *Joule* 1, 480 (2017).
15. G. Zhu, P. Bai, J. Chen, and Z.L. Wang, *Nano Energy* 2, 688 (2013).
16. T.C. Hou, Y. Yang, H. Zhang, J. Chen, L.J. Chen, and Z.L. Wang, *Nano Energy* 2, 856 (2013).
17. N. Zhang, C. Tao, X. Fan, and J. Chen, *J. Mater. Res.* 32, 1628 (2017).
18. J. Chen, G. Zhu, W. Yang, Q. Jing, P. Bai, Y. Yang, and Z.L. Wang, *Adv. Mater.* 25, 6094 (2013).
19. F. Yi, L. Lin, S. Niu, P.K. Yang, Z. Wang, J. Chen, Y. Zhou, Y. Zi, J. Wang, Q. Liao, and Y. Zhang, *Adv. Funct. Mater.* 25, 3688 (2015).
20. Z. Lin, J. Yang, X. Li, Y. Wu, W. Wei, J. Liu, J. Chen, and J. Yang, *Adv. Funct. Mater.* 28, 1704112 (2018).
21. C. Yan, W. Deng, L. Jin, T. Yang, Z. Wang, X. Chu, H. Su, J. Chen, and W. Yang, *ACS Appl. Mater. Interfaces* 10, 41070 (2018).
22. K. Meng, J. Chen, X. Li, Y. Wu, W. Fan, Z. Zhou, Q. He, X. Wang, X. Fan, Y. Zhang, and J. Yang, *Adv. Funct. Mater.* 29, 1806388 (2019).
23. N. Zhang, J. Chen, Y. Huang, W. Guo, J. Yang, J. Du, X. Fan, and C. Tao, *Adv. Mater.* 28, 263 (2016).
24. J. Chen, Y. Huang, N. Zhang, H. Zou, R. Liu, C. Tao, X. Fan, and Z.L. Wang, *Nat. Energy* 1, 1 (2016).
25. Y. Peng, J. Chen, A.Y. Song, P.B. Catrysse, P.C. Hsu, L. Cai, B. Liu, Y. Zhu, G. Zhou, D.S. Wu, and H.R. Lee, *Nat. Sustain.* 1, 105 (2018).
26. L. Cai, A.Y. Song, W. Li, P.C. Hsu, D. Lin, P.B. Catrysse, Y. Liu, Y. Peng, J. Chen, H. Wang, and J. Xu, *Adv. Mater.* 30, 1802152 (2018).
27. L. Cai, A.Y. Song, P. Wu, P.C. Hsu, Y. Peng, J. Chen, C. Liu, P.B. Catrysse, Y. Liu, A. Yang, and C. Zhou, *Nat. Commun.* 8, 1 (2017).
28. B. Kumar, B.K. Kaushik, and Y.S. Negi, *J. Mater. Sci. Mater. Electron.* 25, 1 (2014).
29. W. Yang, J. Chen, Q. Jing, J. Yang, X. Wen, Y. Su, G. Zhu, P. Bai, and Z.L. Wang, *Adv. Funct. Mater.* 24, 4090 (2014).
30. Q. Jing, G. Zhu, P. Bai, Y. Xie, J. Chen, R.P. Han, and Z.L. Wang, *ACS Nano* 8, 3836 (2014).
31. L. Jin, J. Chen, B. Zhang, W. Deng, L. Zhang, H. Zhang, X. Huang, M. Zhu, W. Yang, and Z.L. Wang, *ACS Nano* 10, 7874 (2016).
32. S.Y. Kuang, J. Chen, X.B. Cheng, G. Zhu, and Z.L. Wang, *Nano Energy* 17, 10 (2015).
33. B. Zhang, J. Chen, L. Jin, W. Deng, L. Zhang, H. Zhang, M. Zhu, W. Yang, and Z.L. Wang, *ACS Nano* 10, 6241 (2016).
34. J. Chen, J. Yang, Z. Li, X. Fan, Y. Zi, Q. Jing, H. Guo, Z. Wen, K.C. Pardel, S. Niu, and Z.L. Wang, *ACS Nano* 9, 3324 (2015).
35. W. Yang, J. Chen, G. Zhu, X. Wen, P. Bai, Y. Su, Y. Lin, and Z. Wang, *Nano Res.* 6, 880 (2013).
36. H. Zhang, Y. Yang, Y. Su, J. Chen, K. Adams, S. Lee, C. Hu, and Z.L. Wang, *Adv. Funct. Mater.* 24, 1401 (2014).
37. X. Feng, V. Marcon, W. Pisula, M.R. Hansen, J. Kirkpatrick, F. Grozema, and K. Müllen, *Nat. Mater.* 8, 421 (2009).
38. Z.L. Wang, J. Chen, and L. Lin, *Energy Environ. Sci.* 8, 2250 (2015).
39. W. Liu, J. Chen, Z. Chen, K. Liu, G. Zhou, Y. Sun, M.S. Song, Z. Bao, and Y. Cui, *Adv. Energy Mater.* 7, 1701076 (2017).
40. K. Liu, B. Kong, W. Liu, Y. Sun, M.S. Song, J. Chen, Y. Liu, D. Lin, A. Pei, and Y. Cui, *Joule* 2, 1857 (2018).
41. J. Wan, J. Xie, X. Kong, Z. Liu, K. Liu, F. Shi, A. Pei, H. Chen, W. Chen, J. Chen, and X. Zhang, *Nat. Nanotechnol.* 14, 705 (2019).
42. D. Gupta, M. Katiyar, and D. Gupta, *Org. Electron.* 10, 775 (2009).
43. B. Kumar, B.K. Kaushik, and Y.S. Negi, *J. Vac. Sci. Technol. B Nanotechnol. Microelectron. Mater. Process. Meas. Phenom.* 13, 012401 (2013).
44. S.M. Xu, X. Liang, X.Y. Wu, S.L. Zhao, J. Chen, K.X. Wang, and J.S. Chen, *Nat. Commun.* 10, 1 (2019).
45. J. Yang, J. Chen, Y. Su, Q. Jing, Z. Li, F. Yi, X. Wen, Z. Wang, and Z.L. Wang, *Adv. Mater.* 2, 1316 (2015).
46. P. Bai, G. Zhu, Q. Jing, J. Yang, J. Chen, Y. Su, J. Ma, G. Zhang, and Z.L. Wang, *Adv. Funct. Mater.* 24, 5807 (2014).
47. Z. Lin, J. Chen, X. Li, Z. Zhou, K. Meng, W. Wei, J. Yang, and Z.L. Wang, *ACS Nano* 11, 8830 (2017).
48. D. Li and L.J. Guo, *J. Phys. D Appl. Phys.* 41, 105115-1 (2008).
49. D. Threm, J.L. Gugat, A. Pradana, M. Rädler, J. Mikat, and M. Gerken, *IEEE Photonics Technol. Lett.* 24, 912 (2012).
50. P.D. Yang, *Nature* 425, 243 (2013).
51. B.K. Kaushik, B. Kumar, S. Prajapati, and P. Mittal, Organic Thin-Film Transistor Applications: Materials to Circuits (CRC Press, 2016).
52. B. Ruhstaller, T. Beierlein, H. Riel, S. Karg, J.C. Scott, and W. Riess, *IEEE J. Sel. Top. Quantum Electron.* 9, 723 (2003).
53. B. Ruhstaller, S.A. Carter, S. Barth, H. Riel, W. Riess, and J.C. Scott, *J. Appl. Phys.* 89, 4575 (2001).
54. B. Lamprecht, T. Abel, E. Kraker, A. Haase, C. Konrad, M. Tscherner, and T. Mayr, *Phys. Status Solid-R* 4, 157 (2010).
55. P. Mittal, Y.S. Negi, and R.K. Singh, *J. Semicond.* 35, 124002 (2014).
56. P. Bai, G. Zhu, Z.H. Lin, Q. Jing, J. Chen, G. Zhang, J. Ma, and Z.L. Wang, *ACS Nano* 7, 3713 (2013).
57. W. Yang, J. Chen, G. Zhu, J. Yang, P. Bai, Y. Su, Q. Jing, X. Cao, and Z.L. Wang, *ACS Nano* 7, 11317 (2013).
58. J. Yang, J. Chen, Y. Yang, H. Zhang, W. Yang, P. Bai, Y. Su, and Z.L. Wang, *Adv. Energy Mater.* 4, 1301322 (2014).
59. K. Meng, S. Zhao, Y. Zhou, Y. Wu, S. Zhang, Q. He, X. Wang, Z. Zhou, W. Fan, X. Tan, and J. Yang, *Matter* (2020). https://doi.org/10.1016/j.matt.2019.12.025.
60. H. Shirakawa, E.J. Louis, A.G. MacDiarmid, C.K. Chiang, and A.J. Heeger, *J. Chem. Soc. Chem. Commun.* 16, 578 (1977).
61. A. Tsumura, H. Koezuka, and T. Ando, *Appl. Phys. Lett.* 49, 1210 (1986).
62. J.H. Schon and B. Batlogg, *J. Appl. Phys.* 89, 336 (2001).
63. C. Liu, X. Liu, T. Minari, M. Kanehara, and Y.Y. Noh, *J. Inf. Display* 19, 71 (2018).
64. C.W. Tang and S.A. Vanslyke, *Appl. Phys. Lett.* 51, 913 (1987).
65. P.A. Haigh, Z. Ghassemlooy, I. Papakonstantinou, and H. Le Minh, *IEEE Photonics Technol. Lett.* 25, 1687 (2013).
66. B. Geffroy, P. Le Roy, and C. Prat, *Polym. Int.* 55, 572 (2006).
67. B. Kumar, B.K. Kaushik, Y.S. Negi, and V. Goswami, *Microelectron. Reliab.* 54, 100 (2014).

68. G.G. Malliaras and J.C. Scott, *J. Appl. Phys.* 85, 7426 (1999).
69. K. Müllen and U. Scherf, John Wiley & Sons (2006).
70. C. Yun, H. Cho, T.W. Koh, J.H. Kim, J.W. Kim, Y. Park, and S. Yoo, *IEEE Trans. Electron Devices* 59, 159 (2012).
71. K. Guo, J. Zhang, T. Xu, X. Gao, and B. Wei, *J. Display Technol.* 10, 642 (2014).
72. H. Chen, J. Chen, C. Qiu, B.Z. Tang, M. Wong, and H.S. Kwok, *IEEE J. Sel. Top. Quantum Electron.* 10, 10 (2004).
73. Y.M. Kim, J.W. Lee, J.H. Jung, K.K. Paek, M.Y. Sung, J.K. Kim, and B.K. Ju, *IEEE Electron Device Lett.* 27, 558 (2006).
74. H. Choukri, A. Fischer, S. Forget, S. Chenais, T. Billeton, M.C. Castex, and P. Maisse, in *IECON 2006-32nd IEEE Annual Conference on Industrial Electronics* (2006), p. 4865.
75. H. Yang, Y. Zhao, J. Hou, and S. Liu, *Microelectron. J.* 37, 1271 (2006).
76. Y. Ohmori, H. Kajii, and Y. Hino, *J. Display Technol.* 3, 238 (2007).
77. Z. Wu, H. Guo, and J. Wang, *Microelectron. J.* 38, 686 (2007).
78. H. Tetsuka, T. Ebina, T. Tsunoda, H. Nanjo, and F. Mizukami, *Jpn. J. Appl. Phys.* 47, 1894 (2008).
79. Y.S. Tsai, S.H. Wang, F.S. Juang, S.W. Chang, C.H. Chen, M.H. Chung, and T.C. Liao, *J. Display Technol.* 6, 279 (2010).
80. Y. Yim, J. Park, and B. Park, *J. Display Technol.* 6, 252 (2010).
81. L. Lu, J. Yu, L. Long, F. Yu, J. Zhang, H. Zhang, and B. Wei, *Phys. Status Solidi (a)* 208, 2321 (2011).
82. Y. Chen, J. Chen, D. Ma, D. Yan, L. Wang, and F. Zhu, *Appl. Phys. Lett.* 98, 114 (2011).
83. L. Chen, Y. Jiang, H. Nie, R. Hu, H.S. Kwok, F. Huang, and B.Z. Tang, *ACS Appl. Mater. Interfaces* 6, 17215 (2014).
84. C.A. Mills, F.L.M. Sam, A.S. Alshammari, L.J. Rozanski, N.G. Emerson, and S.R.P. Silva, *J. Display Technol.* 10, 125 (2014).
85. N. Zhou, S. Wang, Y. Xiao, and X. Li, *J. Lumin.* 196, 40 (2018).
86. Q. Zheng, D. Qu, Y. Zhang, W. Li, J. Xiong, P. Cai, and X. Zhang, *Opt. Laser Technol.* 101, 85 (2018).
87. Y.H. Huang, B.T. Liou, J.D. Chen, and Y.K. Kuo, *IEEE Photonics Technol. Lett.* 23, 480 (2011).
88. X.W. Zhang, L.M. Liu, J. Li, L. Zhang, X.Y. Jiang, Z.L. Zhang, and X.Y. Liu, *J. Display Technol.* 7, 515 (2011).
89. Y.M. Xie, Q. Sun, T. Zhu, L.S. Cui, F. Liang, S.W. Tsang, and L.S. Liao, *Org. Electron.* 55, 1 (2018).
90. Y.L. Chang and Z.H. Lu, *J. Display Technol.* 9, 459 (2013).
91. S.W. Wen, M.T. Lee, and C.H. Chen, *J. Display Technol.* 1, 90 (2005).
92. A. Fischer, S. Chénais, S. Forget, M.C. Castex, D. Ades, A. Siove, and B. Geffroy, *J. Phys. D Appl. Phys.* 39, 917 (2006).
93. C.C. Lee, C.H. Yuan, S.W. Liu, and Y.S. Shih, *J. Display Technol.* 7, 454 (2011).
94. K.J. Bergemann, R. Krasny, and S.R. Forrest, *Org. Electron.* 13, 1565 (2012).
95. F. Li, Y. Zhang, C. Wu, Z. Lin, B. Zhang, and T. Guo, *Vacuum* 86, 1895 (2012).
96. C.H. Gao, X.B. Shi, D.Y. Zhou, L. Zhang, Z.K. Wang, and L.S. Liao, *Int. J. Photoenergy* 2013, 1 (2013).
97. H. Li, Y. Tao, R. Chen, H. Li, L. Chen, Y. Jiang, and W. Huang, *Dyes Pigm.* 151, 187 (2018).
98. H.C. Chen, C.P. Kung, W.G. Houng, Y.R. Peng, Y.M. Hsien, C.C. Chou, C.J. Kao, T.H. Yang, and J. Hou, *IEEE/OSA J. Display Technol.* 5, 216 (2009).
99. M. Hack and J.J. Brown, *Inf. Display* 20, 12 (2004).
100. M.S. Weaver, V. Adamovich, M. Hack, R. Kwong, and J.J. Beown, in *Proc. Int. Conf. Electroluminescence of Molecular Materials and Related Phenomena*, Korea, O-35 (2003).
101. P. Mittal, B. Kumar, Y.S. Negi, B.K. Kaushik, and R.K. Singh, *Microelectron. J.* 43, 985 (2012).
102. D. Ammermann, A. Böhler, S. Dirr, H.H. Johannes, and W. Kowalsky, *Int. J. Electron. Commun.* 50, 327 (1996).
103. H. Riel, S. Karg, T. Beierlein, W. Rieß, and K. Neyts, *J. Appl. Phys.* 94, 5290 (2003).
104. H. Fujikawa, M. Ishii, S. Tokito, Y. Taga, in *Proc. Mater. Res. Soc. Symp.* 621, Q3.4.1. (2000).
105. D.F. O'Brien, P.E. Burrows, S.R. Forrest, B.E. Koene, D.E. Loy, and M.E. Thompson, *Adv. Mater.* 10, 1108 (1998).
106. B.J. Chen, W.Y. Lai, Z.Q. Gao, C.S. Lee, S.T. Lee, and W.A. Gambling, *Appl. Phys. Lett.* 75, 4010 (1999).
107. B. Kumar, B.K. Kaushik, and Y.S. Negi, *J. Comput. Electron.* 13, 627 (2014).
108. T. Mori, in *Lasers and Electro-Optics Society*, 2005. LEOS 2005. The 18th Annual Meeting of the IEEE (2005), p. 585.
109. S. Negi, P. Mittal, and B. Kumar, *Microsyst. Technol.* 24, 4981 (2018).
110. L.S. Hung, C.W. Tang, M.G. Mason, P. Raychaudhuri, and J. Madathil, *Appl. Phys. Lett.* 78, 544 (2001).
111. M.Y. Lim, W.M.M. Yunus, Z.A. Talib, A. Kassim, C.F. Dee, and A. Ismail, *Am. J. Eng. Appl. Sci.* 3 (2010).
112. J. Park, Y. Kawakami, and S.H. Park, *J. Lightwave Technol.* 25, 2828 (2007).
113. J. Park, T. Kim, J. Lee, and D. Shin, *IEEE Photonics Technol. Lett.* 20, 1408 (2008).
114. J.J. Huang, Y.K. Su, F.S. Juang, Y.H. Liu, and S.J.L. Chang, *IEEE Photonics Technol. Lett.* 20, 1784 (2008).
115. Q. Wang, Z. Deng, J. Chen, and D. Ma, *IEEE Trans. Electron Devices* 57, 2221 (2010).
116. T. Dobbertin, M. Kroeger, D. Heithecker, D. Schneider, D. Metzdorf, H. Neuner, E. Becker, H.H. Johannes, and W. Kowalsky, *Appl. Phys. Lett.* 82, 284 (2003).
117. V. Bulovi, V.B. Khalfin, G. Gu, P. Burrows, D.Z. Garbuzov, and S.R. Forrest, *Phys. Rev. B* 58, 3730 (1998).
118. T. Shiga, H. Fujikawa, and Y. Taga, *J. Appl. Phys.* 93, 19 (2003).
119. C.K. Moon, S.Y. Kim, J.H. Lee, and J.J. Kim, *Opt. Express* 23, A279 (2015).
120. W.H. Kim, A.J. Mäkinen, N. Nikolov, R. Shashidhar, H. Kim, and Z. Kafafi, *Appl. Phys. Lett.* 80, 3844 (2002).
121. C.T. Lee, L.Z. Yu, and H.Y. Liu, *IEEE Photonics Technol. Lett.* 22, 272 (2010).
122. J.W. Huh, J. Moon, J.W. Lee, D.H. Cho, J.W. Shin, J.H. Han, and H.Y. Chu, *IEEE Photonics J.* 4, 39 (2012).
123. D. Wahyuningrum and A. Alni, *Procedia Chem.* 16, 586 (2015).
124. E.R. Triboni, M.R. Fernandes, J.R. Garcia, M.C. Carreira, R.G.D.S. Berlinck, P.B. Filho, and M. Cremona, *J. Taibah Univ. Sci.* 9, 579 (2015).
125. F. Krujatz, O. Hild, K. Fehse, M. Jahnel, and A. Werner, *Chem. Sci. J.* 7, 134 (2016).
126. J. Shi and C.W. Tang, *Appl. Phys. Lett.* 80, 3201 (2002).
127. S.W. Culligan, Y. Geng, S.H. Chen, K. Klubek, K.M. Vaeth, and C.W. Tang, *Adv. Mater.* 15, 1176 (2003).
128. C. Hosokawa, H. Higashi, H. Nakamura, and T. Kusumoto, *Appl. Phys. Lett.* 67, 3853 (1995).
129. W.J. Shen, B. Banumathy, H.H. Chen, and C.H. Chen, in *Proceedings of the International Display Manufacturing Conference* (2003), p. 741.
130. Z.Y. Xie, L.S. Hung, and S.T. Lee, *Appl. Phys. Lett.* 79, 1048 (2001).
131. K. Suzuki, A. Seno, H. Tanabe, and K. Ueno, *Synth. Met.* 143, 89 (2004).
132. J. Luo, Y. Zhou, Z.Q. Niu, Q.F. Zhou, Y. Ma, and J. Pei, *J. Am. Chem. Soc.* 129, 11314 (2007).
133. C.W. Tang, S.A. VanSlyke, and C.H. Chen, *J. Appl. Phys.* 65, 3610 (1989).
134. C.W. Ko and Y.T. Tao, *Appl. Phys. Lett.* 79, 4234 (2001).
135. P. Chen, L. Zhao, and Y. Duan, *J. Lumin.* 131, 2144 (2011).
136. H.J. Kim, M.H. Shin, H.G. Hong, B.S. Song, S.K. Kim, W.H. Koo, and Y.J. Kim, *J. Display Technol.* 12, 526 (2016).

137. I. Akimoto, S. Tsuzuki, H. Uzawa, M. Hinatsu, Y. Nishide, H. Osuga, and H. Sakamoto, *Phys. Status Solidi (c)* 8, 124 (2011).
138. J. Kido, K. Hongawa, K. Okuyama, and K. Nagai, *Appl. Phys. Lett.* 64, 815 (1994).
139. J. Kido, M. Kimura, and K. Nagai, *Science* 267, 1332 (1995).
140. M. Li, W. Li, J. Niu, B. Chu, B. Li, X. Sun, and Z. Hu, *Solid-State Electron.* 49, 1956 (2005).
141. B.W. D'Andrade, M.E. Thompson, and S.R. Forrest, *Adv. Mater.* 14, 147 (2002).
142. J. Thompson, R.I.R. Blyth, M. Mazzeo, M. Anni, G. Gigli, and R. Cingolani, *Appl. Phys. Lett.* 79, 560 (2001).
143. Y. Nishide, H. Osuga, K. Iwata, K. Tanaka, and H. Sakamoto, *Bull. Chem. Soc. Jpn.* 81, 1322 (2008).
144. Y. Sun, N.C. Giebink, H. Kanno, B. Ma, M.E. Thompson, and S.R. Forrest, *Nature* 440, 908 (2006).
145. J.H. Seo, J.H. Kim, J.H. Seo, *SID Symposium Digest of Technical Papers* p2-38, 1399 (2007).
146. J.H. Seo and J.H. Park, *Appl. Phys. Lett.* 90, 203507 (2007).
147. B. Kumar, B.K. Kaushik, and Y.S. Negi, *I.E.T. Circuits Devices Syst.* 8, 131 (2014).
148. J. Shi and C.W. Tang, *Appl. Phys. Lett.* 70, 1665 (1997).
149. W. Li, R.A. Jones, S.C. Allen, J.C. Heikenfeld, and A.J. Steckl, *J. Display Technol.* 2, 143 (2006).
150. K. Fehse, K. Walzer, K. Leo, W. Lövenich, and A. Elschner, *Adv. Mater.* 19, 441 (2007).
151. S.I. Na, S.S. Kim, J. Jo, and D.Y. Kim, *Adv. Mater.* 20, 1 (2008).
152. S.F. Tseng, W.T. Hsiao, K.C. Huang, and D. Chiang, *Appl. Phys. A* 112, 41 (2013).
153. B.H. Tong, Q.B. Mei, R.Q. Tian, M. Yang, Q.F. Hua, Y.J. Shi, and S.H. Ye, *RSC Adv.* 6, 34970 (2016).
154. B. Kumar, B.K. Kaushik, Y.S. Negi, S. Saxena, and G.D. Varma, *Microelectron. J.* 44, 736 (2013).
155. H. Klauk, U. Zschieschang, and M. Halik, *J. Appl. Phys.* 102, 074514-1 (2007).
156. J. Puigdollers, C. Voz, I. Martin, A. Orpella, M. Vetter, and R. Alcubilla, *J. Non-Cryst. Solids* 338, 617 (2004).
157. S. Acharya, J.P. Hill, and K. Ariga, *Adv. Mater.* 21, 1 (2009).
158. G. Horowitz, *Adv. Mater.* 10, 365 (1998).
159. H.N. Raval, S.P. Tiwari, R.R. Navan, S.G. Mhaisalkar, and V.R. Rao, *IEEE Electron Device Lett.* 30, 484 (2009).
160. H. Cho, H. Yoon, K. Char, Y. Hong, and C. Lee, *Jpn. J. Appl. Phys.* 49, 05EB08-1 (2010).
161. B. Kumar, B.K. Kaushik, and Y.S. Negi, *J. Comput. Electron.* 12, 765 (2013).
162. J.H. Kim, D.S. Kim, S.K. Kim, Y.Z. Yoo, J.H. Lee, S.W. Kim, and T.Y. Seong, *Ceram. Int.* 42, 3473 (2016).
163. D. Miao, S. Jiang, S. Shang, and Z. Chen, *Vacuum* 106, 1 (2014).
164. Y. Yoo and H.K. Jeong, *Chem. Commun.* 21, 2441 (2008).
165. V.Y. Butko, X. Chi, D.V. Lang, and A.P. Ramirez, *Appl. Phys. Lett.* 83, 4773-1 (2003).
166. D. Kumaki, T. Umeda, T. Suzuki, and S. Tokito, *Org. Electron.* 9, 921 (2008).
167. Y. Yun, C. Pearson, and M.C. Petty, *IET Circuits Devices Syst.* 3, 182 (2009).
168. W. Junfeng, J. Yadong, Y. Yajie, Y. Junsheng, and X. Jianhua, *Energy Procedia* 12, 609 (2011).
169. B. Kaushik, B. Kumar, Y.S. Negi, P. Mittal, in *Advances in Computer Science, Engineering & Applications*, vol. 167 (Springer, Berlin, Heidelberg, 2012), p. 125.
170. C.M. Keum, S. Liu, A. Al-Shadeedi, V. Kaphle, M.K. Callens, L. Han, and R.J. Twieg, *Sci. Rep.* 8, 699 (2018).
171. H.A. Becerril, M.E. Roberts, Z.H. Liu, J. Locklin, and Z.N. Bao, *Adv. Mater.* 20, 2588 (2008).
172. G. Giri, E. Verploegen, S.C. Mannsfeld, S. Atahan-Evrenk, D.H. Kim, S.Y. Lee, and Z. Bao, *Nature* 480, 504 (2011).
173. J.H. Kim, S.T. Williams, N. Cho, C.C. Chueh, and A.K.Y. Jen, *Adv. Energy Mater.* 5, 1401229 (2015).
174. J. Xu, Y. Wang, H. Shan, Y. Lin, Q. Chen, V.A.L. Roy, and Z. Xu, *ACS Appl. Mater. Interfaces* 8, 18991 (2016).
175. C. Grigoriadis, C. Niebel, C. Ruzie, Y.H. Geerts, and G. Floudas, *J. Phys. Chem. B* 118, 1443 (2014).
176. C. Xu, P. Cai, X. Zhang, Z. Zhang, X. Xue, J. Xiong, and J. Zhang, *Sol. Energy Mater. Sol. Cells* 159, 136 (2017).
177. M. Zvarik, D. Martinicky, L. Hunakova, I. Lajdova, and L. Sikurova, *Neoplasma* 60, 533 (2013).
178. Q. Zheng, F. You, J. Xu, J. Xiong, X. Xue, P. Cai, and L. Wang, *Org. Electron.* 46, 7 (2017).
179. M. Faustini, B. Louis, P.A. Albouy, M. Kuemmel, and D. Grosso, *J. Phys. Chem. C* 114, 7637 (2010).
180. M. Le Berre, Y. Chen, and D. Baigl, *Langmuir* 25, 2554 (2009).
181. S. Roland, R.E. Prud'homme, and C.G. Bazuin, *ACS Macro Lett.* 1, 973 (2012).
182. P. Mittal, Y.S. Negi, and R.K. Singh, *Microelectron. Eng.* 150, 7 (2016).
183. P. Mittal, Y.S. Negi, and R.K. Singh, *J. Comput. Electron.* 14, 828 (2015).
184. S. Negi, P. Mittal, and B. Kumar, *IET Circuits Devices Syst.* 13, 1255 (2019).
185. G.G. Malliaras and J.C. Scott, *J. Appl. Phys.* 83, 5399 (1998).
186. J. Chan, A.D. Rakic, Y.T. Yeow, and A.B. Djurisic, in *IEEE Conference on Optoelectronic and Microelectronic Materials and Devices* (2004), p. 53.
187. J. Park and Y. Kawakami, *J. Display Technol.* 2, 333 (2006).
188. P.W.M. Blom, M.J.M. de Jong, and S. Breedijk, *Appl. Phys. Lett.* 71, 930 (1997).
189. Y. Nagata and C. Lennartz, *J. Chem. Phys.* 129, 034709 (2008).
190. C. Pflumm, C. Gartner, and U. Lemmer, *IEEE J. Quantum Electron.* 44, 790 (2008).
191. C. Pflumm, C. Karnutsch, M. Gerken, and U. Lemmer, *IEEE J. Quantum Electron.* 41, 316 (2005).
192. D. Shin, Y. Kim, N. Chang, and M. Pedram, *IEEE Trans. Comput. Aided Des. Integr. Circuits Syst.* 32, 1017 (2013).
193. T.K. Wee and R.K. Balan, in *Proceedings of the first ACM International Workshop on Mobile Gaming* (2012), p. 25.
194. M.S. El-Nasr and S. Yan, in *Proceedings of the 2006 ACM SIGCHI International Conference on Advances in Computer Entertainment Technology, ACE'06* (2006).
195. C.H. Lin, C.K. Kang, and P.C. Hsiu, in *2014 51st ACM/EDAC/IEEE Design Automation Conference (DAC)* (2014), p. 1.
196. Y. Liu, Y. Chen, D. Buso, and G. Zissis, *IEEE Trans. Ind. Appl.* 52, 5219 (2016).
197. J. Jacobs, D. Hente, and E. Waffenschmidt, in *2007 IEEE Industry Applications Annual Meeting* (2007), p. 1147.
198. D. Buso, S. Bhosle, Y. Liu, M. Ternisien, C. Renaud, and Y. Chen, *IEEE Trans. Ind. Appl.* 50, 1459 (2014).
199. R.L. Lin, J.Y. Tsai, D. Buso, and G. Zissis, in *2015 IEEE Industry Applications Society Annual Meeting* (2015), p. 1.
200. C.L. Fan, Y.C. Chen, C.C. Yang, Y.K. Tsai, and B.R. Huang, *J. Display Technol.* 12, 425 (2016).
201. S. Negi, P. Mittal, B. Kumar, and P.K. Juneja, *Microelectron. Eng.* 218, 111154 (2019).
202. K.I. Miyamoto, K. Kaneko, A. Matsuo, T. Wagner, S.I. Kanoh, M.J. Schöning, and T. Yoshinobu, *Sens. Actuators B Chem.* 170, 82 (2012).
203. C.F. Werner, T. Wagner, K.I. Miyamoto, T. Yoshinobu, and M.J. Schöning, *Sens. Actuators B Chem.* 175, 118 (2012).
204. R. Shinar, Z. Zhou, B. Choudhury, and J. Shinar, *Anal. Chim. Acta* 568, 190 (2006).
205. P. Mittal, Y.S. Negi, and R.K. Singh, *J. Comput. Electron.* 14, 360 (2015).
206. E. Manna, T. Xiao, J. Shinar, and R. Shinar, *Electronics* 4, 688 (2015).
207. B.A. Prabowo, Y.F. Chang, Y.Y. Lee, L.C. Su, C.J. Yu, Y.H. Lin, and K.C. Liu, *Sens. Actuators B Chem.* 198, 424 (2014).
208. B. Choudhury, R. Shinar, and J. Shinar, *J. Appl. Phys.* 96, 2949 (2004).

209. J. Vučić, C. Kottke, S. Nerreter, K. Habel, A. Büttner, K.D. Langer, and J.W. Walewski, in *Proc. OFC NFOEC* (2010), p. 1.
210. P.A. Haigh, Z. Ghassemlooy, H. Le Minh, S. Rajbhandari, F. Arca, S.F. Tedde, and I. Papakonstantinou, *J. Lightwave Technol.* 30, 3081 (2012).
211. P.A. Haigh, Z. Ghassemlooy, and I. Papakonstantinou, *IEEE Photonics Technol. Lett.* 25, 615 (2013).